UNIVERSITY OF CALIFORNIA
SANTA CRUZ

INSIGHT INTO CLIMATE VARIATIONS OF THE EARLY MIDDLE EOCENE: HIGH-RESOLUTION BENTHIC STABLE ISOTOPE DATA FROM SITE 1408, NEWFOUNDLAND RIDGE

A thesis submitted in partial satisfaction
of the requirements for the degree of

MASTER OF SCIENCE

In

EARTH AND PLANETARY SCIENCES

By

FEI WU

September 2015

The thesis of Fei Wu
is approved by:

_____
Professor James C. Zachos, Chair

_____
Associate Professor Matthew Clapham

_____
Professor Christina Ravelo

_____
Tyrus Miller
Vice Provost and Dean of Graduate Studies

TABLE OF CONTENTS

Abstract iv

Acknowledgments vi

Chapter I Introduction 1

Climate of the Eocene and unsolved challenges 1

Ocean circulation in the middle Eocene 10

Purpose of this study 12

Site and core description 18

Chapter II Methods 23

Chapter III Results 27

Chapter IV Discussion 42

Early Middle Eocene climate variations 42

Orbital-scale climate variations 45

Eocene bottom water and N. Atlantic circulation 56

Chapter V Conclusions 62

Reference 63

Appendix 68

Table 1 Isotope Data 68

Table 2 Trace Element Data 88

Table 3 Isotopic Run Standard Data 91

Abstract

Fei Wu

Insight into climate variations of the early middle Eocene:
High-resolution benthic stable isotope data from site 1408, Newfoundland Ridge

The middle Eocene is a transitional period from the greenhouse early Eocene to the ice-house Eocene-Oligocene Transition. Due to lack of high-resolution records, the details of this long-term cooling trend are not clear. Low-resolution atmospheric CO_2 records suggest declining, but highly variable levels during the middle Eocene which might have driven transient climate variations. However, high-resolution stable isotope records are lacking to document the true climate patterns over this period. Moreover, orbital scale climate reconstructions are essential for reconciling how the sensitivity to orbital forcing changed, if at all, as the greenhouse boundary conditions changes from the early to late Eocene. High-resolution isotope and trace metal records are also essential for constraining the evolution of northern hemispheric sea-ice and continental glaciation as well as North Atlantic Deep Water in the middle Eocene.

To address these shortcomings, I have generated high-resolution stable isotope and trace element data for a site in the northern Atlantic on Newfoundland Ridge (IODP, Site 1408). The records span Chron20r (46.4~43.8 Ma), and are the first orbital-scale stable isotope records for the early middle Eocene. With the exception of the uppermost portion of the section, the $\delta^{18}O$ data indicate gradual cooling of

0.8~1.2 ^{o}C/Myr over much of the section from 46.4Ma to 44.3 Ma which is consistent with the long-term global cooling trend. This is accompanied by a decrease in Mg/Ca records, while the paired δ^{18}O-Mg/Ca analysis shows no pronounced shift in $\delta^{18}O_{sw}$ implying no variation in ice volume. In the upper part of the section (44.3~43.8 Ma), the δ^{18}O shows a slight reversal consistent with warming, while Mg/Ca proxy indicates a continuous cooling. One hypothesis for the apparent between the two records is that the water mass reflects changes in the salinity of local bottom water and a possible shift toward a higher-latitude, cooler and less salty water source. In addition, clear astronomically paced cycles are observed in the stable isotopic and lithological records, and spectral analysis demonstrate that the cycles are dominated by 41-kyr obliquity cycles, a unique feature of Paleocene-Eocene records which are typically dominated by precession and eccentricity. This could reflect either shift in orbital configuration (low eccentricity signals or change in Earth's tilt), or gradual climatic variation toward the ice-house world in the middle Eocene. Interbasin δ^{13}C gradient reveals relatively low δ^{13}C values at this northern Atlantic site compared with records from the Southern Ocean, indicating the meridional circulation was northward and/or North Atlantic Deep Water formation was absent or weak during this time.

Acknowledgements

First of all, I would like to thank to my supervisor James Zachos, who is not only a top scientist in the field of paleoclimatology, but also an excellent advisor to his students. I learned massive knowledge in my research area as well as the way to do research from his guidance. His patient and precious editing is of huge assistance for this thesis. Not a word is sufficient to express my gratitude to Jim.

I would like to express my gratitude to my committee members Ana Ravelo and Matthew Clapham for their valuable advice which significantly improved the drafting of the final thesis.

I would like to thank to Donald Penman, Dustin Harper and Tali Babila for valuable suggestions for data analysis through discussion. Don was also in the crew of this expedition program to collect the sediments for this research.

I am indebted to Colin Carney and Dyke Andreasen in the Stable Isotope Laboratory. Their dedicated manipulation helped me generate the over 900 stable isotope records with high accuracy.

I also would like to thank to Walker Weir, Nicolette Lawler, Gabriel Gordan and Cheyne Hirota who worked in Zachos Lab in their senior years. Without their assistance in sample processing, I could not generate all these data in such a short time frame.

Introduction

1.1 Climate of the Eocene and unsolved challenges

The Eocene epoch (55.8-33.7 Ma) was climatically one of the most dynamic periods in Earth history. It began with gradual warming peaking with the ice-free extreme greenhouse conditions of the early Eocene climatic optimum (EECO) followed by a long-term transition to the ice-house world and onset of Antarctic glaciation at the Eocene-Oligocene transition (EOT) (Figure 1). The long-term trends were interrupted by transient events, short-lived warmings and coolings, as well as abrupt steps. The initial Eocene warming was marked by several transient hyperthermal events accompanied by carbon isotope excursions (Lourens et al. 2005, Galeotti et al. 2010) including the Paleocene-Eocene Thermal Maximum (PETM), an episode of extreme global warming and ocean acidification suggestive of a massive carbon release. (e.g. Dickens et al. 1995, Zeebe et al. 2009). The long-term warming phase reached a sustained peak lasting a few million years, the EECO, which terminated around 49 Ma with an initial abrupt phase of cooling that gradually continued into the early middle Eocene (Norris et al. 2001). Over the middle Eocene, the cooling trend was temporarily interrupted by the Middle Eocene Climatic Optimum (MECO, ~40 Ma). By the late Eocene, the gradual cooling eventually led to the rapid appearance of large scale continental ice-sheets at the

Figure 1. Reconstructions of pCO_2 (a), $\delta^{13}C$ (b) and $\delta^{18}O$ (c) for the period 30 to 60 Ma (Zachos et al., 2008). The Eocene epoch is between the PETM event at 55 Ma and the EOT at 33 Ma. Atmospheric CO_2 data are from compilation of both marine and lacustrine proxy records (Pearson and Palmer, 2000; Pagani et al.,2005), showing a general decrease over the Cenozoic period, though with considerable variability in the middle Eocene. Deep sea benthic foraminiferal stable isotope data are from the global compilation of Zachos (et al., 2008). Isotope data from multiple species (*N.truempyi, Cibcidoides spp.*) with species specific adjustments. The temperature is derived from $\delta^{18}O$ assuming ice-free $\delta^{18}O_{sw}$ of -1.2‰. The $\delta^{13}C$ values are generally stable in the middle Eocene, while $\delta^{18}O$ is indicated by a long-term increase trend, representing long trend cooling. The cooling trend may be suspended at around 44 Ma, which requires support from records with higher resolution.

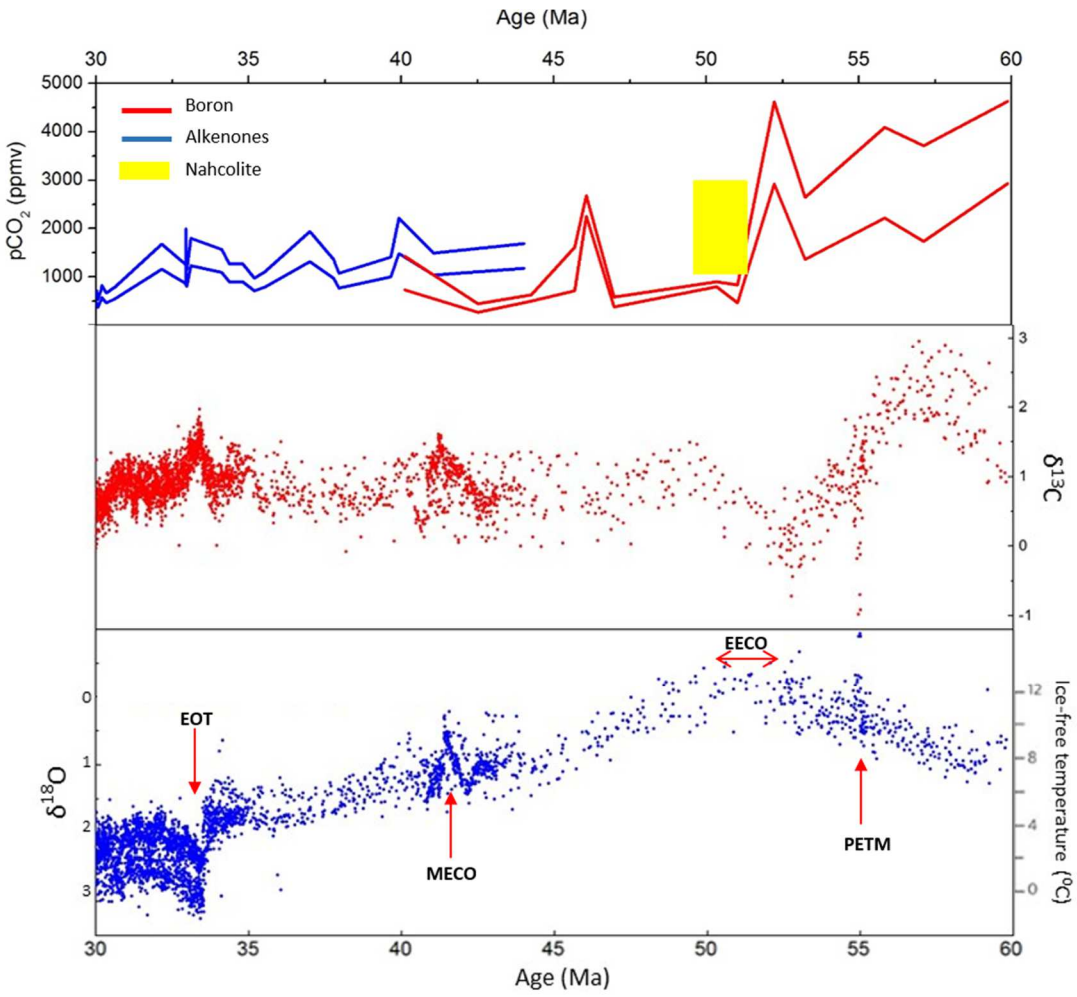
Age (Ma)
30
35
40
45
50
55
60
5000
4000
3000
2000
1000
pCO2 (ppmv)
Boron
Alkenones
Nahcolite
3
2
1
0
-1
δ13C
EECO
EOT
MECO
PETM
δ18O
0
1
2
3
12
8
4
0
Ice-free temperature (ºC)
Age (Ma)

Eocene-Oligocene Transition (EOT, ~34 Ma) (e.g. Coxall et al. 2005, Bohaty et al. 2012) and a uniform drop in ocean T of 2-3^{o}C. The exact triggers for the excursions and rapid transitions remains questionable, though new evidence suggests they likely involve thresholds and carbon cycle feedbacks.

In order to better understand the nature of the transitions, and excursions, significant effort has gone into characterizing variability on orbital time scales for specific segments of the Eocene. The successful development of such records for key segments of the Eocene have been instrumental in unraveling the mechanisms triggering the major climatic changes of the Eocene, particularly the transient events and even abrupt transitions. Much of the focus of these high-resolution studies has been on the early and late Eocene, and have revealed an overall shift in the sensitivity of the climate system to orbital forcing. Over the early Eocene, the primary power in paleoclimate records is concentrated in the precession and eccentricity bands (Zachos et al., 2010; Littler et al. 2014). In addition, the hyperthermal events appear to coincide with 100-kyr and/or 405-kyr maximum in eccentricity, which is preferential for extreme seasonality and increased seawater temperature in both hemispheres (Lourens et al. 2005), thus providing a triggering mechanism for oceanic methane hydrate release at the onset of the PETM and other hyperthermals, ETM2 (Elmo) and ETM3 ('X').

By the end of the Eocene, power in the response of the climate system builds in the obliquity bands. This is particularly pronounced across the EOT and through the Oligocene (Palike et al. 2006). In fact, computations of earth's orbit and analysis of oxygen isotope records suggest a rare confluence of Low amplitude eccentricity and obliquity oscillations roughly coincident with the onset of the EOT, combined with gradually declining pCO_2, resulting in an extended period of cooler summers, thus benefitting snow accumulation and subsequent expansion of ice-sheets (Coxall et al. 2005).

While much progress has been achieved in establishing the detailed climate patterns of the early and late Eocene, reconstructions of a key transition interval, the early- middle Eocene (i.e., Chrons 20 -21) are of insufficient resolution to delineate even the most basic features of the onset of cooling and how forcing factors, including orbital variations, contributed to climate evolution of this interval. The few existing high-resolution records from the early – middle Eocene are typically of poor quality, often short, truncated, and/or with gaps. One of the more complete records, from Site 1258 in the equatorial Atlantic, suggests that orbital configuration of the early middle Eocene is dominated by precession cycles which are modulated by 100-ky and 400-ky eccentricity, while strong obliquity signals with weak eccentricity are observed only ephemerally in Chron22r (Westerhold and Rohl, 2009). The short-term strengthening of obliquity roughly coincided with the onset of long-term global cooling, and this unique strong obliquity has been interpreted as

reflecting stronger ocean and atmosphere circulation which transported high-latitude signals to the low-latitudes. Orbital-scale paleoclimate reconstruction for Site 1258 based on lithologic cycles in C20r-C18r also reveals dominant precession and eccentricity signals while the obliquity cycles are not pronounced (Westerhold & Rohl, 2013). However, comparable data from other locations are lacking and thus temporal extension of orbital-scale climatic changes are limited by lack of orbital-resolution sediment records.

Efforts to constrain the contributions of greenhouse forcing to these Eocene transitions are progressing. Reconstructions of pCO_2 using boron isotope or $\delta^{13}C$ of di-unsaturated alkenones show a general decline of pCO_2 through the Eocene (Pearson et al. 2009, Pagani et al. 2005, e.g.), coincident with the decline in global temperature. However, the reconstructions contain large uncertainties in the absolute range of values, as well as in the approximate timing. This is particularly true for the early middle Eocene during which one of the proxies, B isotopes, suggests a dramatic drop in pCO_2 of a magnitude that should have triggered Antarctic glaciations. (ref) And yet, evidence for such glaciation has yet to be documented, in large part for the lack of detailed deep sea oxygen isotope and other paleoclimatic records spanning this interval.

A key issue regarding middle Eocene climate is the conflicting evidence for the presence or absence of continental ice-sheets. Traditionally, large scale Cenozoic

glaciation is thought to have initiated on Antarctica during the EOT while northern hemisphere glaciation did not initiate until Neogene. However, this view has recently been challenged by several lines of evidence. Sediment drifts indicating that small-scale transient glaciation and sea-ice appeared early in the middle Eocene in Northern Hemisphere (Figure 2). Dropstones have been reported from the Arctic in sediments at ~45 Ma, suggesting the existence of seasonal sea ice in the early middle Eocene. (Backmann et al., 2005), and ice-margin diatoms in the Arctic site 302 indicate seasonal sea ice as early as 48 Ma (Stickley et al., 2009). In addition, studies on the provenance of iron grains in marine sediments from the central Arctic suggest that perennial sea ice originated ~44 million years ago (Darby 2014). This agrees with the results of coupled global climate–ice sheet model experiments that suggest that glaciers and small isolated ice caps could have been present at high elevations in the North Hemisphere through much of the Cenozoic, but that major continental-scale glaciation prior to the Miocene was unlikely (Deconto et al. 2008).

These direct constraints on glaciation are contradicted to some extent by several studies utilizing deep sea isotope constraints on middle Eocene ice volume. With a range of assumed $\delta^{18}O_{ice}$, observed changes of $\delta^{18}O$ from benthic foraminifera in equatorial Pacific and Atlantic sites are converted to ice volume changes, which indicate that large-scale glaciation could not exist in the middle Eocene though the possibility of small glaciers in the northern hemisphere cannot be

Figure 2. Distribution of geological evidence for the presence and timing of northern hemisphere ice in the middle/late Eocene. Evidence for the earliest continental glaciation existed at 38 Ma, and evidence for sea ice extend to the early middle Eocene.

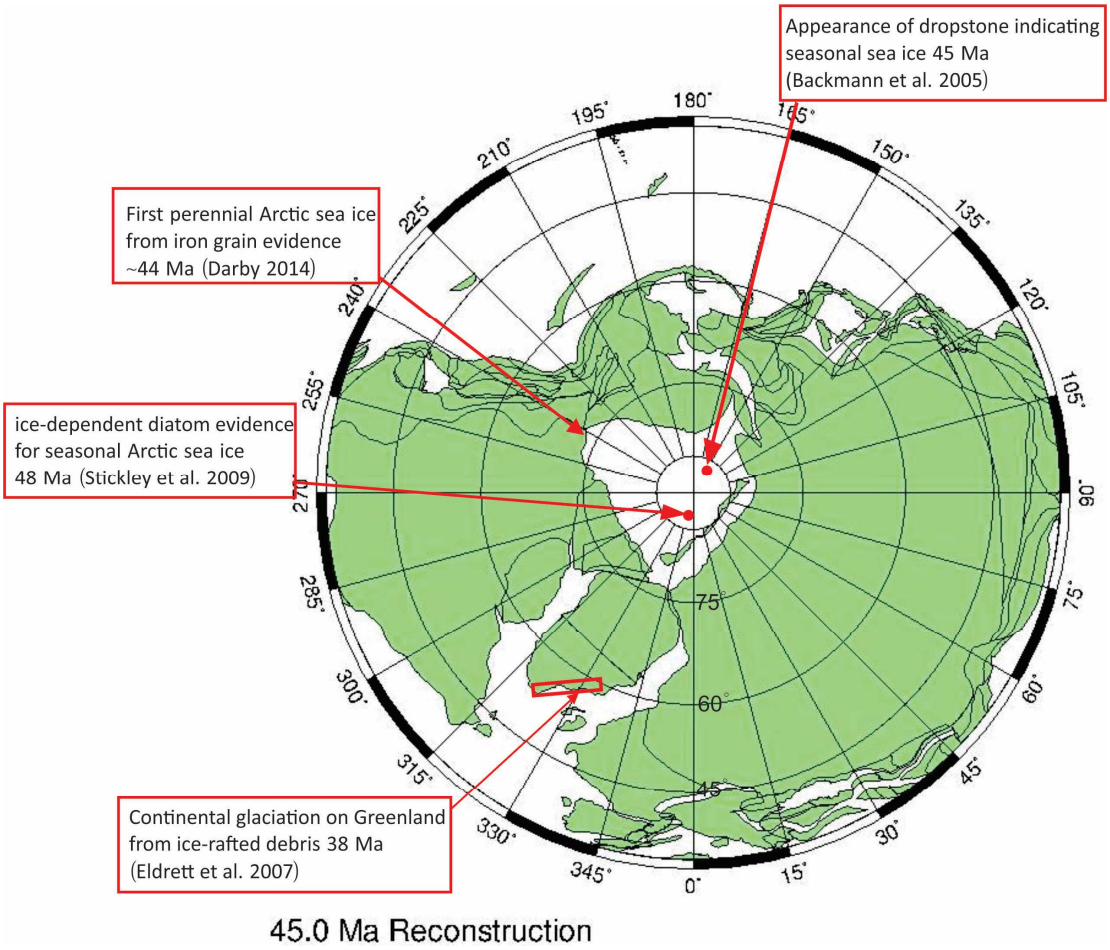

45.0 Ma Reconstruction

excluded around 41.6 Ma (Edgar et al. 2007). The lack of evidence, however, is insufficient proof against the presence of ice-sheets, as there are few sedimentary sections spanning the early middle Eocene, and most lack the resolution to detect small scale or transient ice sheets.

1.2 Ocean circulation in the middle Eocene

In the modern ocean, the meridional overturning circulation (MOC) is primarily dominated by deep water formation in the North Atlantic, while the Southern Ocean also contributes through Antarctic Bottom Water Formation. However, with the differences in basin configuration and gateways and reduced meridional temperature gradients, a different mode has been demonstrated to exist in the early Eocene with deep water formation dominated by the Southern Ocean regions. Climate models forced under Eocene greenhouse conditions always generate southern sourced bottom waters, but not North Atlantic Deep Water, at least not routinely (e.g., Huber et al., 2004). Isotope and other records confirm the presence of young bottom waters in the southern ocean (Zachos et al., 1992b; Cramer et al. 2011). The presence of northern component deep water in the Paleogene remains unclear, however, for lack of sufficient data coverage (Wright and Miller, 1993). Multiple studies utilizing a variety of proxies have been attempted to constrain the history of North Atlantic sourced bottom waters. Recent studies of

sediment drifts in Greenland-Scotland Ridge, which is the gateway between Norwegian-Greenland Sea and the Northern Atlantic, suggest the onset of North Atlantic Deep Water was coincident with the initiation of climatic cooling in the Eocene (Hohbein et al. 2012). Reconstructions of Nd isotope variations in the southeastern Atlantic Ocean indicate that the initial transition to a bipolar mode of deep-water circulation occurred in the early Oligocene resulting from the tectonic deepening of the sill separating the Greenland-Norwegian Sea from the North Atlantic (Via and Thomas, 2006).

To resolve the ocean circulation pattern, benthic foraminiferal $\delta^{13}C$ records have also been used to assess circulation patterns. Interbasin $\delta^{13}C$ gradients, as recorded by benthic foraminifera, reflect on water mass flow paths and ageing as sinking organic matter is remineralized, releasing isotopically light carbon into sub-surface waters (Curry and Oppo, 2005). This process produces the modern interbasin $\delta^{13}C$ pattern with the most enriched values in the N. Atlantic and most depleted values in the deep Pacific. In the Paleogene, the interbasin $\delta^{13}C$ patterns indicate weak or reversed gradients relative to the modern suggesting a lack of significant deep water formation in the North Atlantic. During the early middle Eocene, low-resolution benthic foraminiferal $\delta^{18}O$ and $\delta^{13}C$ data from multiple sites suggest an increase in interbasin gradient coincident with the termination of EECO which indicate a shift from a homogenous ocean to significant deep water originating in the Southern Ocean (Sexton et al. 2006). However, the site locations

are not ideal for establishing the deep water chemical gradients, particularly near the current region of NADW formation. The records generated by this study for the high-latitudinal Atlantic will thus be critical in establishing the northern end-member water chemistry, and thus the flow direction and possibly the strength of Atlantic ocean circulation.

1.3 Purpose of this study

Our knowledge of the climatic variations in the Eocene epoch has improved with the recovery and study of deep sea cores during the recent two decades. However, as outlined in the preceding review of Eocene climate dynamics, one of the least understood intervals is the middle Eocene, particularly the interval spanning 45 to 40 Ma (C20r – C19r) which represents the initial phase of the long-term cooling. The cyclostratigraphy of C20r has been generated based on 405-kyr eccentricity extraction from bulk $\delta^{13}C$ records tuned to orbital eccentricity solution Laskar2011. (Figure 3, Westerhold et al., 2015) Questions concerning the detailed temperature variations, ocean circulation pattern, pCO_2 level and the history of ice-sheets on both and short-time scales still remain unsolved. This study is designed to address some of these critical issues, specifically related to the character of orbital scale climate variability of climate during the early middle Eocene. Here I present new data from a ~2.5 Myr interval spanning ~43.8-46.3 Ma (Chron 20r) from site

Figure 3. Early- middle Eocene (C19r-C21r) cyclostratigraphy generated using high-resolution bulk $\delta^{13}C$ data for ODP Sites 1263 and 702 (Westerhold et al., 2015). The 405-kyr (in black) eccentricity was extracted by Gaussian filtering. Both records indicate low eccentricity during C20r which is the time interval of this study.

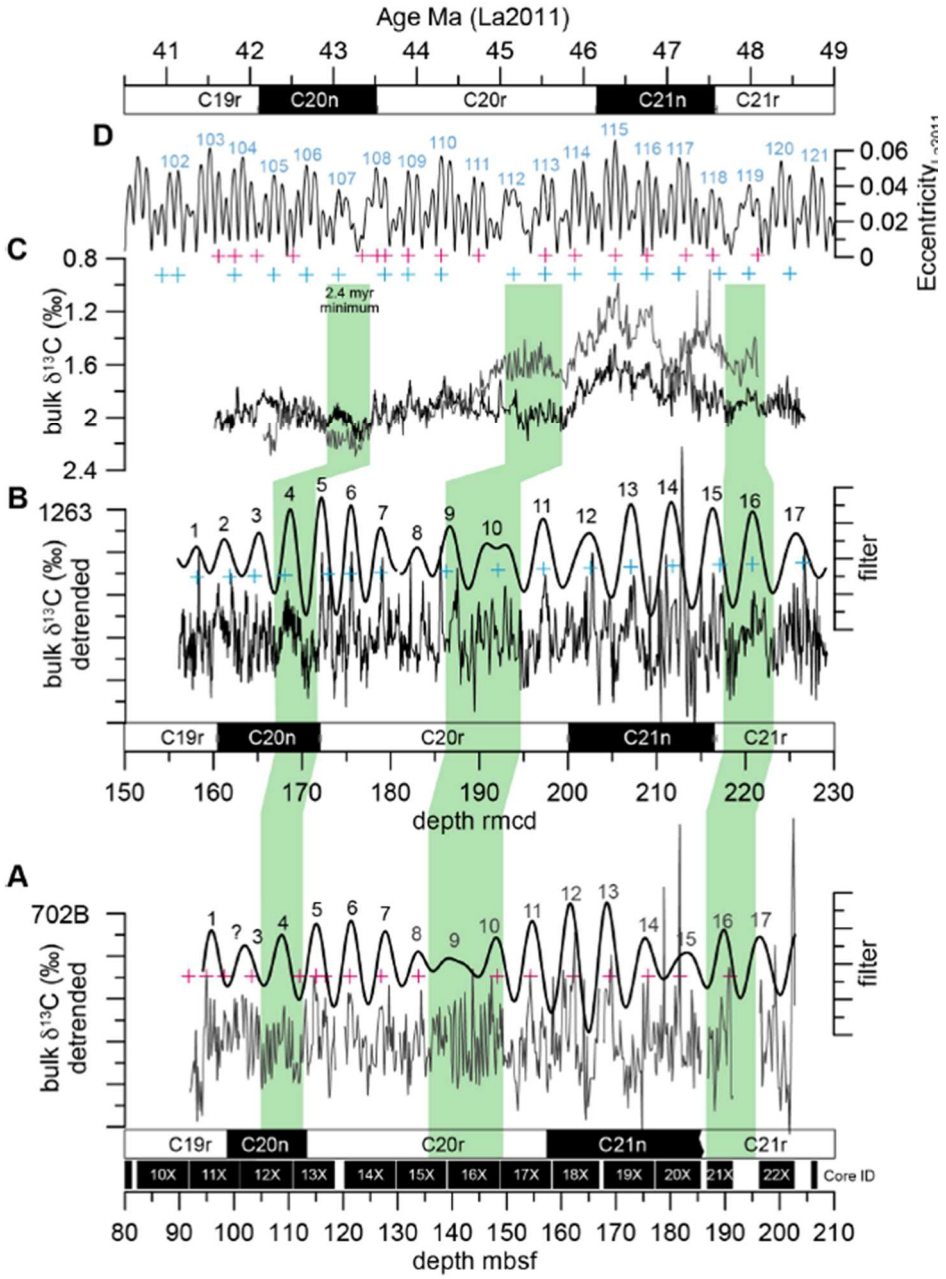
Age Ma (La2011)
41 42 43 44 45 46 47 48 49
C19r C20n C20r C21n C21r
D
Eccentricity
0.06 0.04 0.02 0
C
bulk δ13C (‰)
0.8 1.2 1.6 2 2.4
2.4 myr minimum
B
bulk δ13C (‰) detrended
1263
filter
C19r C20n C20r C21n C21r
150 160 170 180 190 200 210 220 230
depth rmcd
A
702B
bulk δ13C (‰) detrended
filter
C19r C20n C20r C21n C21r
10X 11X 12X 13X 14X 15X 16X 17X 18X 19X 20X 21X 22X
Core ID
80 90 100 110 120 130 140 150 160 170 180 190 200 210
depth mbsf

1408, a mid-depth site cored on Newfoundland Rise in the western North Atlantic during Integrated Ocean Drilling Program (IODP) Expedition 342. As with other sites from this region, site 1408 is characterized by high sedimentation rates (~2.8 cm/kyr) enabling resolution of orbital cycles in core logging and other data, both shipboard and shore-based. I generated orbital-scale benthic $\delta^{18}O$ and $\delta^{13}C$ records on this interval based on analyses of *N. truempyi* a common foraminiferal species. To constrain bottom water temperature and carbonate saturation state, I generated lower resolution Mg/Ca and B/Ca records, also based on analyses of *N. truempyi*. I compare these data to Ca/Fe data generated by X-ray fluorescence (XRF) core scanning to gain additional insights into the climatic and geochemical evolution of the ocean in this region and globally. I find periodic cycles superposed on more gradual trends in the isotope records. Detailed spectral analysis of my data reveal distinct high-frequency cycles with periods matching those of the orbital cycles. Notably, the 41-ky obliquity cycles dominate the proxy records while precession cycles are weak throughout most of the studied section. To reconstruct general patterns of the MOC, I also compare the site 1408 benthic isotope records to records from other sites in the Atlantic and other ocean basins.

Figure 4. Bathymetric map showing the location of IODP site 1408. Site 1408 is located on the Southeast Newfoundland Ridges in western North Atlantic. Modern water depth of site 1408 is 3022 m and the paleodepth is ~2575 m at 50 Ma. Blue arrows indicate the pathways of modern Deep Western Boundary Current (DWBC).

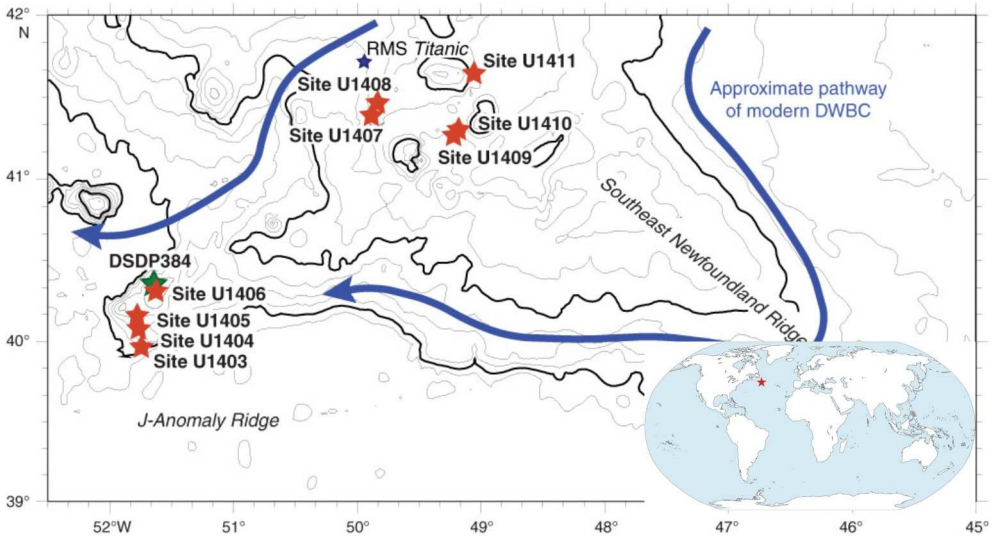
42° N
41°
40°
39°
52°W
51°
50°
49°
48°
47°
46°
45°
RMS Titanic
Site U1411
Site U1408
Site U1407
Site U1410
Site U1409
Approximate pathway of modern DWBC
Southeast Newfoundland Ridge
DSDP384
Site U1406
Site U1405
Site U1404
Site U1403
J-Anomaly Ridge

1.4 Site and core description

Integrated Ocean Drilling Program Expedition 342 cored nine sites (1403-1411) along the southern flank of J-Anomaly Ridge and the slopes of seamounts on Southeast Newfoundland Ridge, in the North Atlantic (Figure 4). The J-Anomaly and Southeast Newfoundland Ridges formed along the axis of the mid-Cretaceous Mid-Atlantic Ridge, the tops of both ridges were above sea level in the Aptian and subsequently subsided to abyssal depths by the Late Cretaceous. This expedition was designed to recover Paleogene sedimentary sequences with unusually high deposition rates across a wide range of water depths. In terms of the location along the flow path of the Deep Western Boundary Current in the northwest Atlantic Ocean, sedimentary and geochemical records from the drilling sites should capture the history of the Deep Western Boundary Current.

Site 1408 is a mid-depth site located on the Southeast Newfoundland Ridges with ~3022 m modern water depth and paleodepth of ~2575 m at 50 Ma. Site 1408 is composed of three holes (Hole A, B and C) with Hole B 20 m east of Hole A, and Hole C 20 m south of Hole B. Cores were retrieved using advanced piston coring (APC) or the extended core barrel (XCB) with high recovery rates. The ~250 m thick sedimentary succession extends from the Pleistocene to late Paleocene, with several hiatuses. The succession is divided into four lithostratigraphic units. The sampled middle Eocene section is in Unit III, a 202 m thick sequence of predominantly

greenish gray nannofossil ooze and clay. It exhibits cyclical color variations between greenish gray to dark green and very light gray intervals on a decimeter-scale.

Samples were taken from the following cores: 1408A-17X~23X, 1408B-19X~25X and 1408C-19H~20X in Unit III, roughly 166 to 238mcd. Both the upper and lower boundaries of the study section are close to the upper and lower boundaries of C20r, implying that the section spans the interval 46.4-43.8 Ma based on CK95 Geomagnetic Polarity Time Scale (GPTS; Cande and Kent, 1995) (Figure 5). Calcareous microfossils indicate that this is within zones NP 15a to NP 15c, and planktonic foraminifera zones E8 to E9. The chronostratigraphy suggest high sedimentation rates of ~2.8 cm/kyr for this interval, which along with the distinct cycles can enable the reconstruction of orbital-scale stable isotope records at the resolution required to resolve precession cycles. Planktonic and benthic foraminifers are common in this interval. Foraminifer shells, both planktonic and benthic, in the clay-rich Eocene sediments are well-preserved, as indicated by glassy, translucent textures, unfilled tests, with detailed surface ornamentation.

The current splice for the three holes was determined by high-resolution magnetic susceptibility data collected during the expedition. However, the signal amplitude is weak in the lower end of my records, resulting in several mis-alignments, and rendering the current splice unreliable. To improve the splices, stable isotope data from bulk carbonate and planktonic foraminifera will eventually

be applied to test and adjust alignments. For the time being, this limits the ability to tune the records and assess the orbital scale variability in a robust fashion.

Figure 5. Stratigraphic summary for Site 1408 from the Preliminary report of Expedition 342. Core recovery, lithology, biostratigraphy and magnetic stratigraphy are shown in this figure. Yellow areas indicate the sampled section in this study, which nearly spans the full length of Chron20r. As a continuous record from a single hole is not reachable, I apply the splice generated based on XRF data to determine the tiepoints for different holes and establish a continuous sedimentary record for this interval.

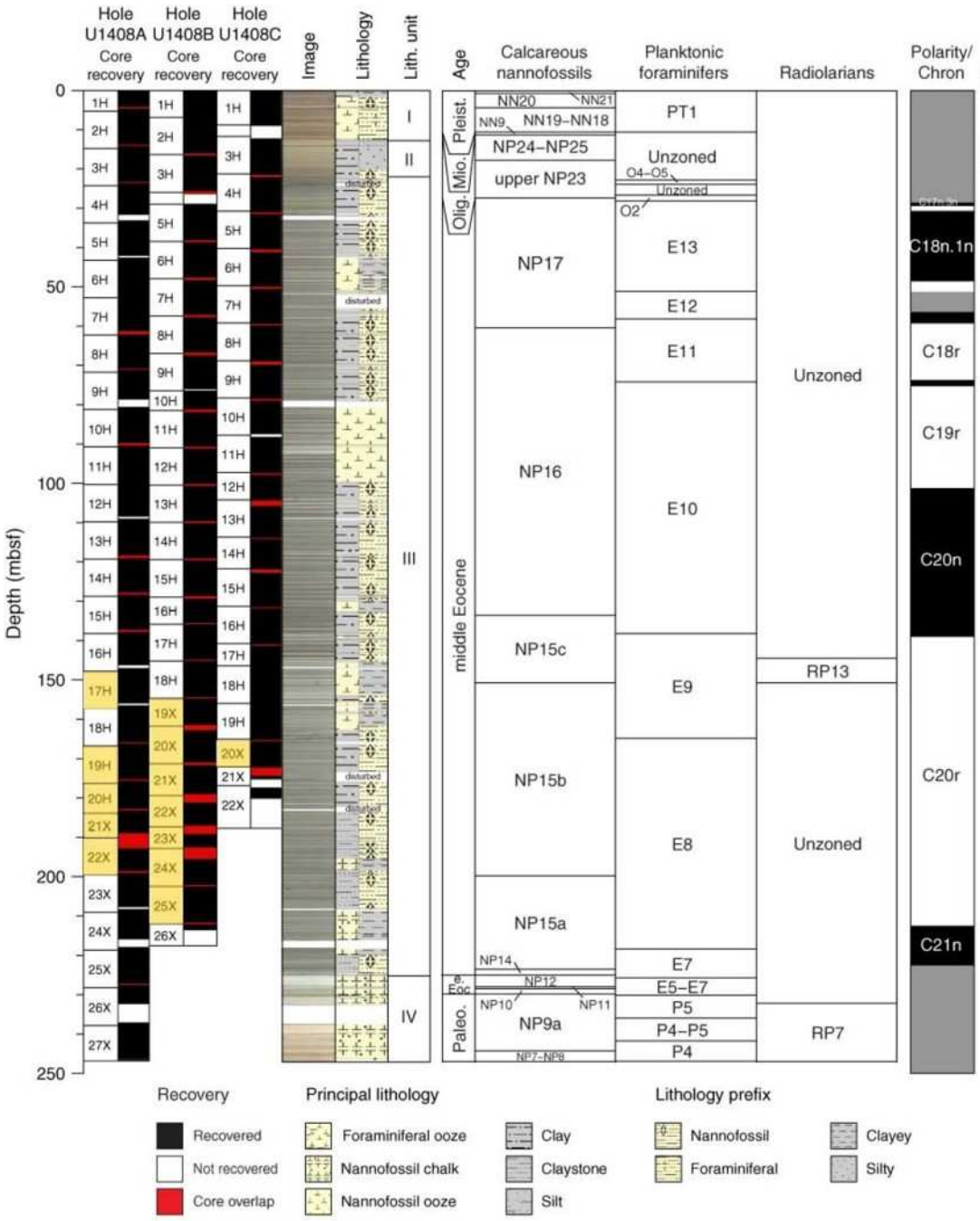
Hole U1408A
Core recovery
Hole U1408B
Core recovery
Hole U1408C
Core recovery
Image
Lithology
Lith. unit
Age
Calcareous nannofossils
Planktonic foraminifers
Radiolarians
Polarity/ Chron
Depth (mbsf)
0
50
100
150
200
250
I
II
III
IV
Pleist.
Mio.
Olig.
middle Eocene
Paleo.
NN20
NN21
NN9
NN19–NN18
NP24–NP25
upper NP23
NP17
NP16
NP15c
NP15b
NP15a
NP14
NP12
NP10
NP11
NP9a
NP7–NP8
PT1
Unzoned
O4–O5
O2
E13
E12
E11
E10
E9
E8
E7
E5–E7
P5
P4–P5
P4
Unzoned
RP13
Unzoned
RP7
C18n.1n
C18r
C19r
C20n
C20r
C21n
disturbed
Recovery
Recovered
Not recovered
Core overlap
Principal lithology
Foraminiferal ooze
Nannofossil chalk
Nannofossil ooze
Clay
Claystone
Silt
Lithology prefix
Nannofossil
Foraminiferal
Clayey
Silty

Methods

2.1 Sample preparation

Samples were taken every 6 cm, representing an age resolution of 2.1 kyrs based on average sedimentation rate of 2.8 cm/kyr. Each 20 cc sediment sample was disaggregated and sieved for extraction of benthic foraminiferal shells, which were generally well preserved, lacking any evidence of overgrowths. The most abundant benthic foraminiferal species are *Nuttallides truempyi* and *Cibicidoides eoceanus*. For the isotope records, *N.truempyi* were selected as their distribution is most continuous across the study interval with common to high abundance. Sediments were disaggregated by soaking in a prepared solution for 24 hrs. The solution consists of 20g sodium metaphosphate dissolved in 1000g distilled water, with ammonia used to adjust pH value to 7.0-7.5. After wet sieving through a 63 μm mesh, the remaining material was soaked in calgon solution again and shook under 200 rpm for 2 hrs. Samples were wet sieved through a 63 μm a second time to remove clay fraction, and residual coarse fraction was air dried in room temperature. Dry weight was recorded to calculate weight percentage of coarse fraction. *N.truempyi* were picked for the size fraction of >300 μm and 212-300 μm respectively, and well-preserved *N.truempyi* of 212-300 μm were chosen for isotope analysis. Ideal weight of carbonate material for mass spectrum run was around 40 μg, which requires 3-4 *N.truempyi* individuals with a sonicating step.

2.2 Stable isotope analysis

Stable isotope analyses were carried out in Stable Isotope Laboratory of University of California, Santa Cruz. The samples were analyzed for $\delta^{18}O$ and $\delta^{13}C$ by phosphoric acid digestion using an individual vial acid drop ThemoScientific Kiel IV carbonate device interfaced to a MAT-253 dual-inlet isotope ratio mass spectrometer. Results are reported in per mil notation (‰) relative to the Vienna Pee Dee Belemnite (VPDB). A calibrated in-house standard Carrara Marble 12, NBS-18 limestone standards and NBS-19 standards were included in each sample run for drift correction and assessing precision, as well as to correct for instrument specific source ionization effects. NBS-19 standards were also sun as samples for quality control and to assess long-term performance. Based on standards within each run, overall precision is better than ±0.08 and 0.05‰ for $\delta^{18}O$ and $\delta^{13}C$, respectively.

2.3 Elemental analysis

Trace element analyses were carried out on *N.truempyi*. A total of 90 samples were chosen for analysis of Mg, B, and Ca. To obtain at least 200 μg of materials, >20 shells of 212~300 μm fraction or >15 shells of >300 μm were picked for each sample. In the lower portion of the section, shells were combined for several successive samples with similar stable isotope ratios to to obtain sufficient material for the weight requirement of trace element analysis. Oxidative-reductive

cleaning followed the procedures in Barker (et al., 2003) to remove clay, organic matter and Mn-oxides respectively. B/Ca and Mg/Ca ratios were measured using an inductively coupled plasma mass spectrometer (ICPMS), the Element XR, at University of California, Santa Cruz. External precision is ±4% for Mg/Ca and ±7% for B/Ca analysis based on long-term running reproducibility.

2.4 Lithologic Cycles and the Shipboard Splice

The Ca/Fe data, generated by XRF core scanner at Bremen University (courtesy S. Kirtland-Turner), are used as a general indicator of lithological variations, specifically the relative concentration of carbonate to clay (Figure 6). Throughout the sampled section, there is a pronounced cyclicity in the Ca/Fe with wavelengths ranging from 0.8 to 1.2 m. The record is also characterized by an abrupt transition from low amplitude (less than 0.5) cycles in the lower part of the record, to high amplitude cycle in the upper portion.

The Ca/Fe records were constructed with samples from a composite splices of three individual holes (Hole A, B, C), and thus used to revise the shipboard splices. Typically, peaks with strong amplitude are used as tie points, as they are more distinguishable than peaks with normal amplitude. However, the amplitude of XRF variations is extremely low in most of my study section, particularly in the lower end of the section, which produces difficulty in properly aligning the core splices. As such, I used the stable isotope records to test the splices. Presumably, the stable

isotope values of overlapped splices should exhibit similar trends and values if all the splices are linked correctly. In this way, I discovered some misalignments mainly concentrated at the middle and lower end of my section. I also examined core photos to check the splice. The color of the sediment varies with the proportion of clay and carbonate, as clay fraction shows dark color while carbonate is white. Comparison of the variations of color among holes confirmed that the alignments in the upper part (44.5~43.8 Ma) are correct. However, the color variations in the lower part are difficult to detect in core photos due to low amplitude lithological cycles. Therefore, I apply the original splice for this study, and use only samples of Hole B when misalignments are observed between two holes.

Results

3.1 Stable isotope records

Given the low amplitude of the lithologic cycles in the lower middle Eocene and related issues with core splicing, the process of developing orbitally tuned age models for the Paleogene in the Expedition 342 sites though underway, will take another year to complete. Therefore, the age model is based on an assumption of a constant sedimentation rate within C20R. The Site 1408 benthic foraminiferal $\delta^{13}C$ and $\delta^{18}O$ records plotted against both mcd and age in Figure 6. The records, which consist of ~800 data points each, are fairly continuous with the exception of one short sampling gap (203 to 198 Mcd). The section is sub-divided into three intervals (I through III) on the basis of major changes in geochemical trends or cycle patterns.

Over the long-term, 46.4 to 43.8 Ma, the $\delta^{18}O$ shows subtle long-term trends with superimposed high frequency cycles, and no abrupt shifts. In interval I, from 237 mcd (46.4 Ma) to 203 mcd (45.3 Ma), the average $\delta^{18}O$ values are characterized by a slight increasing trend, with overall change of less than ~0.1‰. In interval II, from 198 mcd (45.1 Ma) to 183 mcd (44.5 Ma), the trend of rising values continues, but with relatively higher amplitude cycles. Mean values increase from ~0.4‰ to ~0.55‰ in this interval. Interval III, from 44.4 Ma to the top of the study section, the trend reverses with mean $\delta^{18}O$, decreasing from 0.55‰ at 44.4 Ma to 0.25‰ at 43.8 Ma. This reversal coincides with the shift from low to high amplitude cycles in the

Ca/Fe record. (Figure 7) The Site 1408 $\delta^{13}C$ record shows generally low variability over both long and short time scales, with mean values ranging from 0.0‰ to 0.3‰. In interval I, $\delta^{13}C$ data are stable at ~0.2‰, while in interval II values increase by ~0.1‰, coinciding with the rise in $\delta^{18}O$. In interval III, coincident with the reversal in $\delta^{18}O$, the $\delta^{13}C$ data decreased to 0.0‰.

3.2 Spectral Analysis

Spectral and cross spectral analysis of the stable isotope records were performed utilizing the Blackman-Tukey method using Analyseries 2.0 (Paillard et al., 1996), and robust red noise background is applied for the significance calculation. Using the coarse age model generated in this study, my analysis of the isotope time series reveals a dominant obliquity signal (Figure 8). A small peak is also resolved near the 100-ky eccentricity frequency, whereas a 400-ky eccentricity signal is not present. The precession signals are not pronounced, though this might reflect on issues with the age model. Cross spectral analysis indicates strong coherency at obliquity for $\delta^{13}C$, $\delta^{18}O$ and log(Ca/Fe) in the lower section (Interval I) whereas the coherency in the upper section is weaker despite higher amplitudes (Figures 11, 12)

Figure 6. Benthic foraminiferal (*N. truempyi*) $\delta^{13}C$ (in red), $\delta^{18}O$ (in blue) records for site 1408 with log(Ca/Fe) records (in green) from XRF data (courtesy of S. Kirtland-Turner) in the studied interval. All data are plotted versus MCD of the lower x-axis, and with the linear age modelon the upper x-axis. The record is sub-divided in three intervals on the basis of changes in trend of $\delta^{18}O$. In interval I, the average $\delta^{18}O$ values are characterized by a slight increasing trend, with overall change of less than ~0.1‰. The $\delta^{13}C$ records are stable over Interval I. Above the gap from 202 to 198 mcd which has not been recovered, the trend of rising values in $\delta^{18}O$ continues , but with relatively higher amplitude cycles in interval II. Mean values increase from ~0.4‰ to ~0.55‰ in this interval. The $\delta^{13}C$ values are indicated by an increase from ~0.2 to ~0.35‰. The increase trend is followed by a reversed decrease of $\delta^{18}O$ in interval III, which drops from 0.55‰ to 0.25‰ at the top of the record. The $\delta^{13}C$ records show large amplitude variations, and the mean value decrease to ~0.25 ‰ at the top.

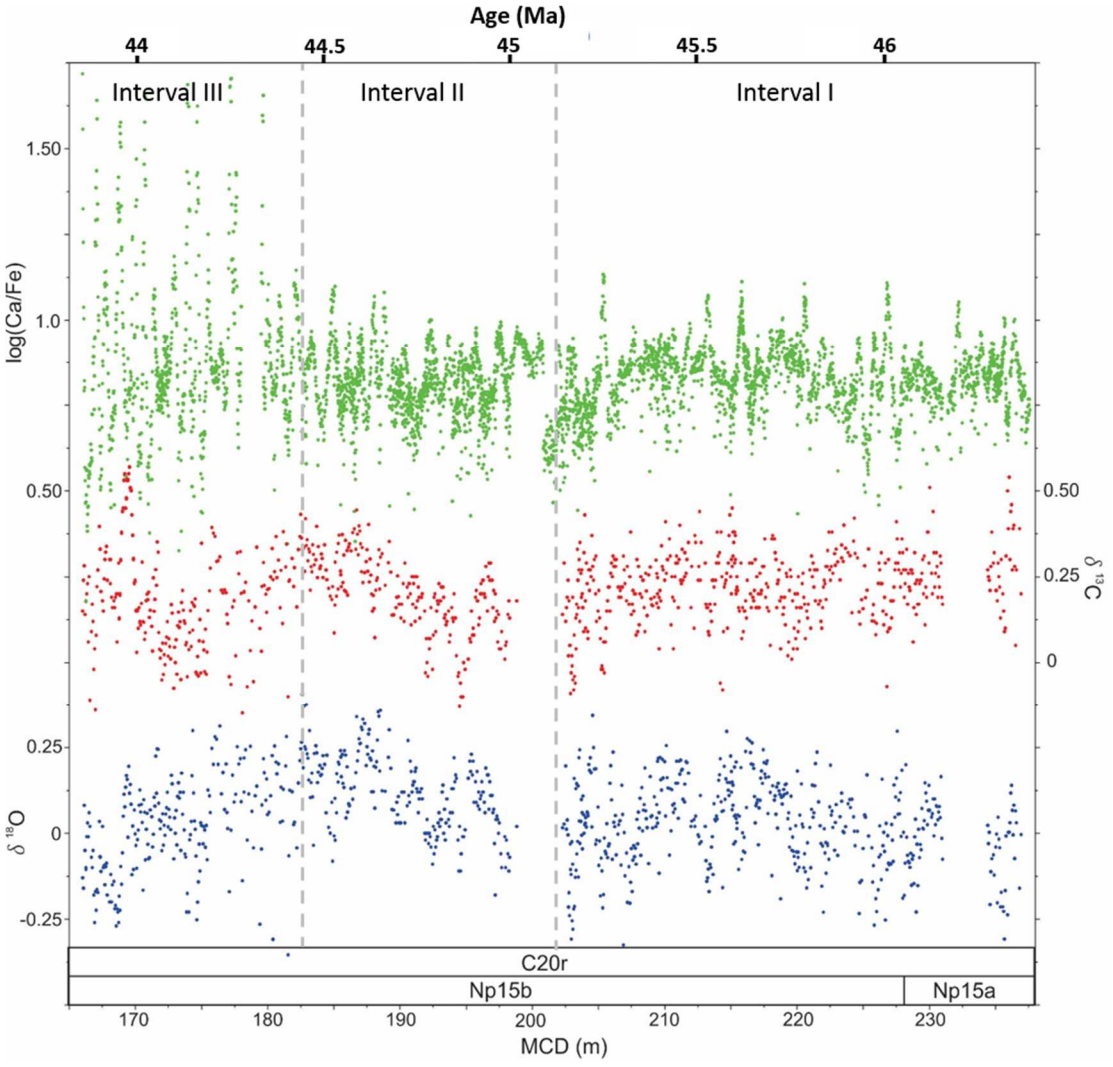
Age (Ma)
44
44.5
45
45.5
46
Interval III
Interval II
Interval I
log(Ca/Fe)
1.50
1.0
0.50
δ 18O
0.25
0
-0.25
δ 13C
0.50
0.25
0
C20r
Np15b
Np15a
170
180
190
200
210
220
230
MCD (m)

Figure 7. Expanded view of interval III and the top of interval II. Benthic foraminiferal (*N. truempyi*) $\delta^{13}C$ (in red), $\delta^{18}O$ (in blue) for site 1408 with log(Ca/Fe) (in green) from XRF data (courtesy of S. Kirtland-Turner) in the studied interval. All data are plotted versus MCD on the lower x-axis. The cyclic patterns of stable isotope are more pronounced compared to the lower part of the study section. The amplitude of variations in log(Ca/Fe) increase abruptly at around 179 mcd.

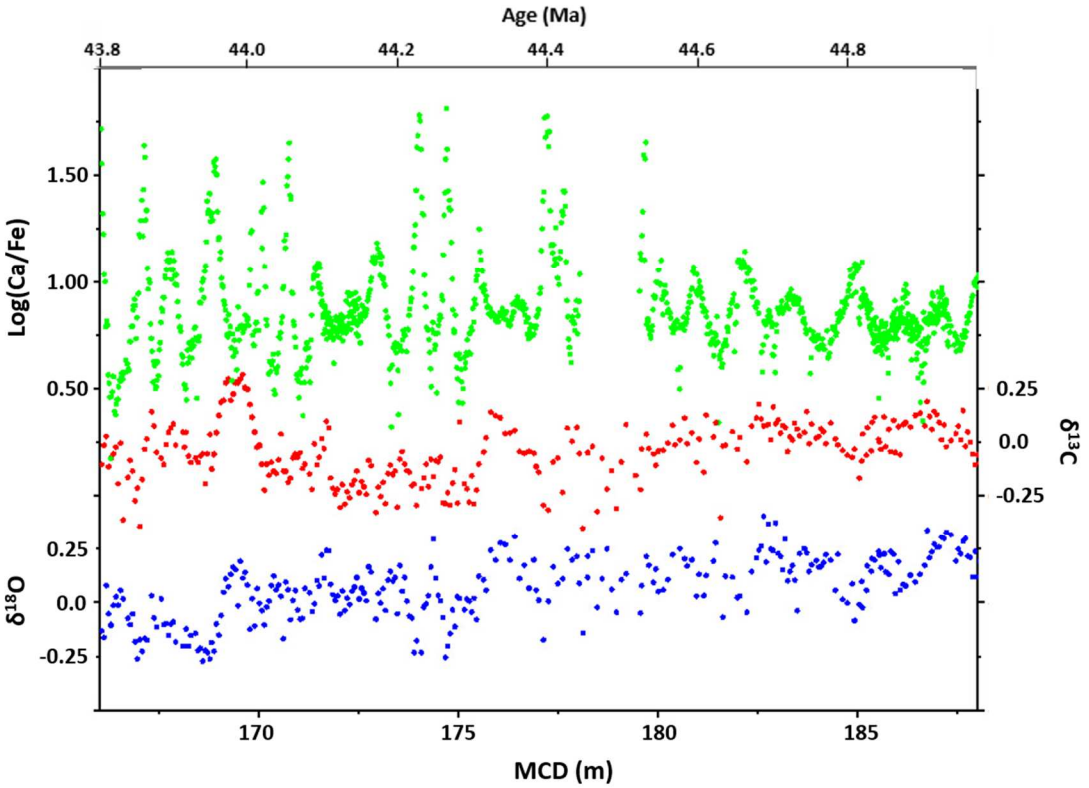
Age (Ma)
43.8
44.0
44.2
44.4
44.6
44.8
Log(Ca/Fe)
1.50
1.00
0.50
δ18O
0.25
0.0
-0.25
δ13C
0.25
0.0
-0.25
170
175
180
185
MCD (m)

Figure 8. Power spectrum of the Site 1408 benthic $\delta^{18}O$ for Interval I based on the Blackman-Tukey method using the software package AnalySeries 2.0 (Paillard et al., 1996). Robust red noise background is applied for the significance calculation. Power is concentrated in the obliquity band with less well-defined power at frequencies associated with 100-kyr eccentricity.

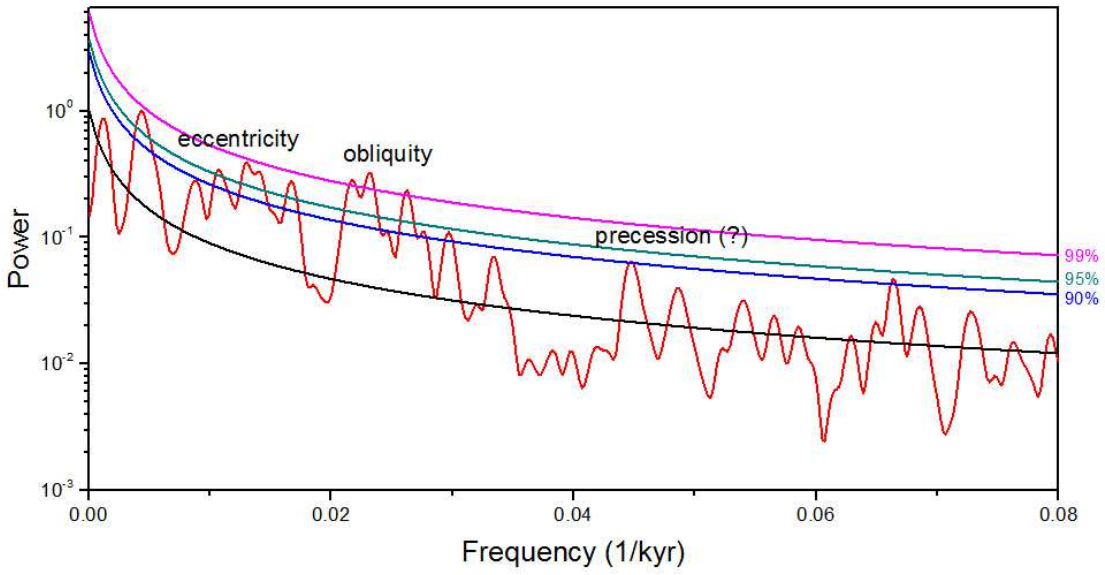
Power
10^{0}
10^{-1}
10^{-2}
10^{-3}
eccentricity
obliquity
precession (?)
99%
95%
90%
0.00
0.02
0.04
0.06
0.08
Frequency (1/kyr)

3.3 Trace Elements

Results of trace element analyses of *N.truempyi* are presented in Figure 9. The Mg/Ca ratio is characterized by a decreasing trend over this period with average Mg/Ca ratio decreasing from 1.8mmol/mol at the bottom of the section to ~1.2 mmol/mol at ~190mcd. Above this, the rate of decrease increases with Mg/Ca ratio 0.8mmol/mol at the top of my section. A higher resolution Mg/Ca record was generated for a short segment from 178mcd to 168mcd, and shows a general correlation of high values in Mg/Ca and lows in $\delta^{18}O$ is observed, while insufficient data points preclude revealing the magnitude of corresponding Mg/Ca and $\delta^{18}O$ correlations. Overall, the *N. truempyi* B/Ca ratios range from 100-140µmol/mol exhibiting no discernible trend up section. The same is true for the short high-resolution segment.

3.4 Conversion of Mg/Ca to temperature

A number of variables need to be constrained or approximated in order to convert Mg/Ca ratios of benthic foraminifera to temperature. To start, variations in seawater Mg/Ca ratio can be significant over geologic time. Second, the partitioning

Figure 9. Site 1408 Benthic foraminiferal oxygen isotope (in blue), Mg/Ca (in black) and B/Ca (in red) records derived from analyses of *N. truempyi*. The Mg/Ca record shows a steady decrease from ~1.6 mmol/mol in the lower end to ~0.8 mmol/mol at the top of this section. The trend in Mg/Ca ratio is consistent with increased $\delta^{18}O$ as these proxies both indicate cooling. However, in Interval I, Mg/Ca ratio continues to decreases with decreased $\delta^{18}O$. This apparent paradox between the two proxies might reflect on changes in seawater chemistry. B/Ca record is relatively constant.

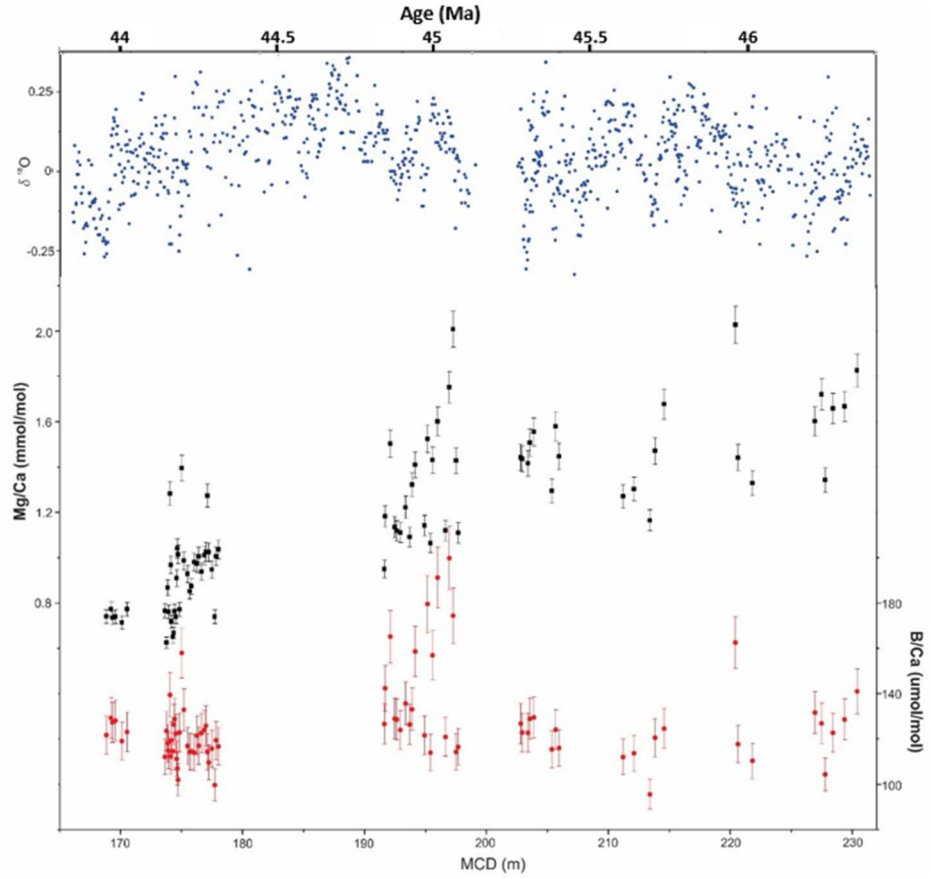
Age (Ma)
44
44.5
45
45.5
46
0.25
0
-0.25
δ 18O
2.0
1.6
1.2
0.8
Mg/Ca (mmol/mol)
180
140
100
B/Ca (umol/mol)
170
180
190
200
210
220
230
MCD (m)

of Mg/Ca between seawater and calcite is sensitive to carbonate ion concentration, particularly when the deep sea temperature is below 4°C (Lear et al. 2002), and when saturation state $\Delta[CO3^{2-}]$ is low, though the threshold varies for different species (Eldrett et al. 2007, Rosenthal et al. 2006). Here, I constrain $\Delta[CO3^{2-}]$ using my B/Ca data and the equation $\Delta[CO3^{2-}]$ = B/Ca-(134±2.7)/(1.23±0.15) (Brown et al. 2011), which suggest negative values for most of the record. I adopt the correction for $\Delta[CO3^{2-}]$ fromYu and Elderfield (2008). Another factor which should be considered for correcting Mg/Ca ratio is Mg/Ca_{sw}. Over short time scales (<1 to 2 myr), the Mg/Ca_{sw} is assumed to be constant, however, over million year time scales changes primarily due to exchange of Ca and Mg during high temperature weathering of ocean basalts with changes in seafloor crust production rate. The modern Mg/Ca_{sw} is 5.2mol/mol (De Villiers and Nelson, 1999), while data from evaporites, and other marine minerals as well as geochemical simulations constrain the Mg/Ca_{sw} ratio of the middle Eocene to be 2-3mol/mol (Coggon and Teagle, 2010; Farkas et al., 2007). Here, I apply a conservative estimate of 3.0 mol/mol for my computation of T. Recently, it is observed that sensitivity to Mg/Ca_{sw} ratio (H) varies among benthic foraminiferal species (*Segev and Erez,* 2006, *Mewes et al.,* 2014). As no calibration exists for *N.truempyi*, I assume a broad range between 0.3 and 1.0 in this study. The corrected Mg/Ca ratio is achieved based on the equation (Cramer et al., 2011):

$$\mathrm{Mg/Ca_{corr}} = \left(\frac{\mathrm{Mg}}{\mathrm{Ca}}_{\mathrm{bf}} - 0.009 \cdot \Delta[\mathrm{CO_3^{2-}}]\right) \cdot \left(\frac{5.2}{3.0}\right)^{\mathrm{H}}$$

N. truempyi is an extinct species and so lacks a field calibrated Mg/Ca-temperature equation. Equations for other species cannot be applied directly as the temperature sensitivity of $Mg/Ca_{truempyi}$ is not well-established. Therefore, I convert the *N. truempyi* Mg/Ca values to that of an extant species *O.umbonatus* by applying an interspecies offset $Mg/Ca_{umbonatus}=1.9Mg/Ca_{truempyi}$ generated by Cramer (et al, 2011). In this way, I can apply the Mg/Ca-temperature equation for *O.umbonatus*. Both exponential and linear Mg/Ca-T equations have been tested, and my comparisons indicates little difference under 10 ^{o}C, though the exponential equations is more accurate at higher T. Here, I apply the equation for *O. umbonatus* generated by Lear (et al., 2002) from core-top calibrations:

$$\frac{Mg}{Ca} = 1.008 \times e^{0.114T}$$

Figure 10. a. Mg/Ca data based on analyses of *N. truempyi*. b, temperature derived from Mg/Ca. Calculation follows the Mg/Ca-T equation for *O.umbonatus* as the initial data are converted to $Mg/Ca_{umbonatus}$ based on the interspecies offset. c. $\delta^{18}O_{sw}$ data generated based on Mg/Ca-derived temperature and $\delta^{18}O$ using the equation $\delta^{18}O_{truempyi} = \delta^{18}O_{sw}$-0.27+(16.1-T)/4.76 (Bemis et al. 1998). A calibration for the interspecies disequilibrium fractionation of $\delta^{18}O$ is applied. As the absolute $\delta^{18}O_{sw}$ values are unknown, I plot $\Delta\delta^{18}O_{sw}$ to represent changes of $\delta^{18}O_{sw}$ over the study section.

The end-members of sensitivity for Mg/Ca_{sw} are represented by red: h=0.3, and black, h=1.0, symbols.

The temperature variations derived from Mg/Ca ratio exhibits a ~3^{o}C decrease over this interval. The $\delta^{18}O_{sw}$ is generally constant between 230m and 190m, however, a significant decrease of over 0.5‰ is observed in Interval I.

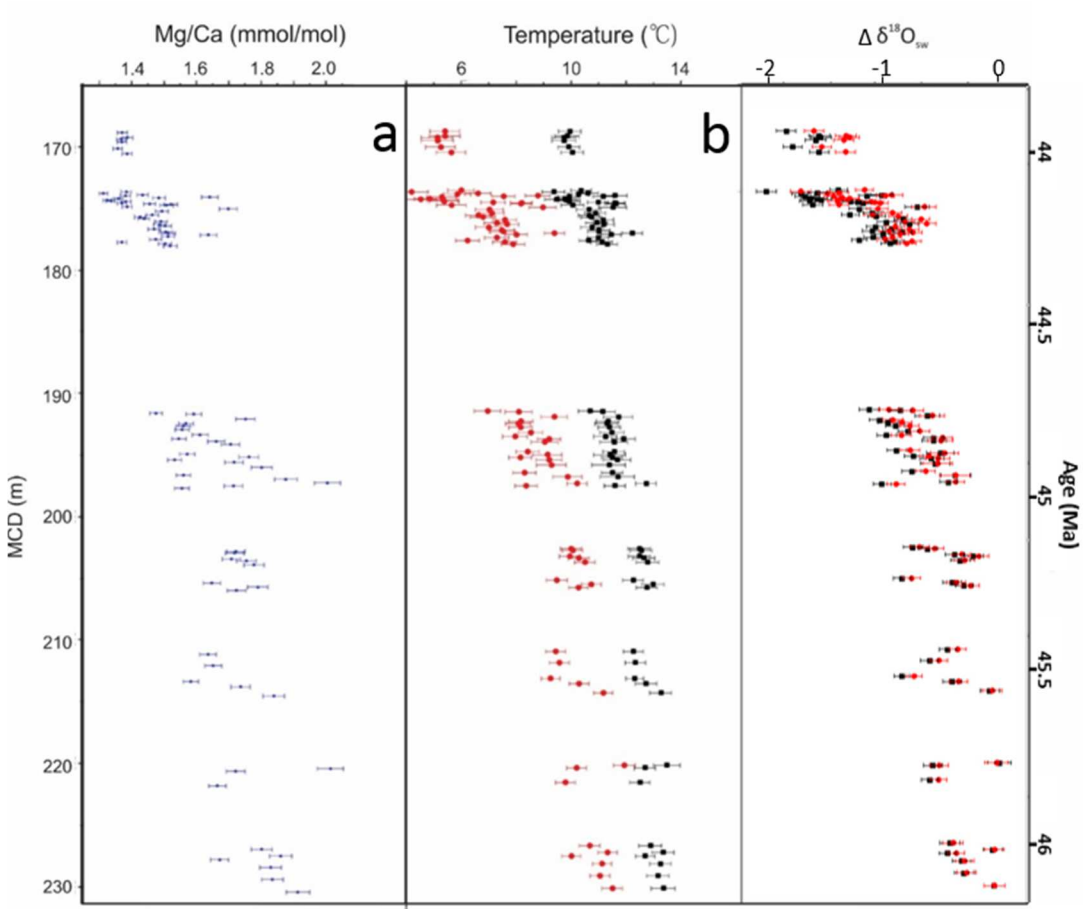
Mg/Ca (mmol/mol)
1.4
1.6
1.8
2.0
Temperature (℃)
6
10
14
Δ δ18Osw
-2
-1
0
a
b
MCD (m)
170
180
190
200
210
220
230
Age (Ma)
44
44.5
45
45.5
46

Discussion

4.1 Early Middle Eocene climate variations

One of the controversial issues regarding Cenozoic climate is whether large ice-sheets existed during the greenhouse Eocene. Claims of middle Eocene glacioeustacy are based mainly on sea level reconstructions using sequence stratigraphic records from passive margins (Miller et al. 1991; 2005). Other evidence, however, including oxygen isotopes and ice rafted debris, has generally not supported such large-scale ice-sheet activity (e.g., Zachos et al., 2001, Edgar et al., 2007). By utilizing the Mg/Ca paleothermometer at Site 1408, I address the question of whether the variations in my benthic $\delta^{18}O$ record are reflecting on changes in seawater $\delta^{18}O_{sw}$, and hence the waxing and waning of ice-sheets.

At Site 1408, the lower portion of the benthic $\delta^{18}O$ records exhibits an increasing trend from 46.4 Ma to ~44.3 Ma, consistent with a global cooling trend in the middle Eocene. Using the $\delta^{18}O$-temperature calibration of Bemis et al (1998). From the total increase of 0.4‰ in the $\delta^{18}O$ records, I estimate a cooling rate of 0.8-1.2 ^{o}C/Myr assuming no change in $\delta^{18}O_{sw}$. The results over this interval are consistent with the general cooling trend in the early middle Eocene as observed in the global $\delta^{18}O$ compilation (Zachos et al. 2001, 2008). The cooling trend, however, appears to not be continuous. Following the long increase in $\delta^{18}O$, the upper part of C20R is characterized by a reversal, and a decrease in $\delta^{18}O$. Closer examination of

the global $\delta^{18}O$ compilation of the middle Eocene also suggests that the long-term cooling terminated around Chron20r, after which $\delta^{18}O$ was stable until the MECO (Bohaty et al., 2003; 2009). The increasing trend of bulk $\delta^{18}O$ from site 702 and site 1263 in the southern Atlantic terminated at around the boundary between C21n and C20r, then stayed constant during C20r. (Westerhold et al., 2015) The timing of this stabilization in the low-resolution global record is close to the reversal in my high-resolution record, suggesting that this warming pattern might be global, but is masked by smoothing in the global compilation.

I then apply Mg/Ca paleothermometer to determine the extent to which the long-term changes in $\delta^{18}O$reflect changes in seawater $\delta^{18}O$ (Figure 9). Due to the uncertainties in correcting the Mg/Ca ratio, the $\delta^{18}O_{sw}$ value derived from Mg/Ca have a large uncertainty. Nevertheless, a stable $\delta^{18}O_{sw}$ trend is observed from 46.4 Ma to 44.3 Ma suggesting no significant long term ice volume change in this period, with the trend in benthic $\delta^{18}O$ representing primarily cooling.

In contrast, in the upper portion of the record after 44.5Ma, where a decrease in $\delta^{18}O$ records indicate a reversal with warming, Mg/Ca records show a continued cooling (Figure 8). Such decoupling of benthic $\delta^{18}O$ and Mg/Ca has been observed previously (Coxall et al., 2005), specifically with the Eocene-Oligocene transition (EOT) for which a large increase in $\delta^{18}O$ is recorded by benthic foraminifera while Mg/Ca is constant. Taken at face value, the decouple of $\delta^{18}O$ and

Mg/Ca at EOT could reflect an increase in ice volume with constant T, possibly due to increased moisture availability in polar areas which enhances precipitation triggering continental glaciation (Lear et al, 2000). Alternatively, because Mg/Ca partitioning in benthic foraminifera is sensitive to carbonate ion concentration, a change in deep sea carbonate ion content offset the trend related to temperature (Rosenthal et al., 1997). Indeed, a substantial deepening of the CCD during the EOT likely increased carbonate ion content to such an extent as to offset the T related change in the partitioning of Mg/Ca (Bohaty et al., 2012).

If the patterns in the Site 1408 records represent global climate signals, this would indicate a significant decrease of ice volume as the oceans cooled. However, as there is no evidence for significant continental glaciation in Antarctica or Greenland prior to the transition, until additional records are generated to test this, I dismiss this scenario. What other possibilities could explain this apparent paradox?

One is that seawater Mg/Ca ratio rapidly decreased during Interval III, which offset the temperature signal. Based on the assumed seawater sensitivity range, a reduction of more than 50% in Mg/Ca_{sw} within 0.5 Myr is required to account for the observed discrepancy. Although the records of the Mg/Ca_{sw} for Eocene are of low resolution, they suggest relatively stable Mg/Ca_{sw} ratios (Coggon and Teagle, 2010, Farkas et al. 2007). Furthermore, reconstructions for crustal production rates also

indicate no abrupt variations during this interval (Muller et al. 2008). Therefore, I dismiss changes in Mg/Ca_{sw} ratio as the primary driver behind this decline in Mg/Ca.

Another possible explanation for the apparent is that the isotopic composition of water masses reaching this site changed, that is reflecting local trends instead of global. During the transition of $\delta^{18}O$ at ~190 mcd, an abrupt shift of water source toward higher latitude occurred, which brought colder and less salty bottom water to this site. This hypothesis would call for a minimum of a 0.5‰ decrease in $\delta^{18}O_{sw}$ with a shift toward higher-latitude source. The modern surface $\delta^{18}O_{sw}$ gradient is almost 2.0‰ between the subtropical and polar regions due to the precipitation-evaporation balance (e.g., Roemmich and Gilson, 2009). During the middle Eocene interval, the gradient might have been more pronounced as the basins were more restricted (ie.gateways were not completely open) and stronger moisture transport toward high latitudes resulted in more precipitation (Scher and Martin, 2006; Huber and Nof, 2006). This supports the possibility that apparent $\delta^{18}O_{sw}$ and Mg/Ca decoupling occurred due to local circulation change, though this model would require additional records to be fully tested.

4.2 Orbital-scale climate variations

Addressing the question of general climate state, the presence or absence of ice-sheets, or the state of ocean circulation can benefit from climate records that

resolve variability on orbital time scales. Until this study, no orbital-scale resolution climate records existed for this interval of the middle Eocene. The high-resolution Site 1408 $\delta^{13}C$, $\delta^{18}O$ and Ca/Fe records all exhibit clear cyclic signals with isochronous variations consistent with response to orbital forcing. To better resolve the character and origin of these cyclical variations I performed spectral analysis on $\delta^{18}O$ and Ca/Fe records (Figure 8). The cyclostratigraphy reveals pronounced obliquity signals throughout records in this study, while the 100-ky eccentricity peaks are also over the 99% confidence level. However, power at precession frequencies is weak. Statistically meaningful resolution of the longer 405-ky eccentricity is precluded by the short length of my sampled section, though if such a low frequency signal were present in either the isotope or Fe/Ca records, the amplitude must be small.

Although no other deep sea climate records exist with the resolution of the Site 1408 record, there are several relatively high resolution lithologic records for various intervals of the early and middle Eocene. Some of those records, from the equatorial and south Atlantic (Demerara Rise and Walvis Ridge), indicate a dominance of eccentricity and precession throughout most of early and middle Eocene period, while obliquity is pronounced only within a short interval coincident with the onset of the long-term cooling trend (Westerhold and Rohl, 2009). Conversely, lithological records from Ainsa basin in Spain, which represent deep-marine siliciclastic facies deposited at ~45 Ma within the section of my study,

despite the absence of a calibrated age model, are dominated by high-amplitude obliquity and less pronounced eccentricity and precession signals (Cantalejo and Pickering, 2015). Similarly, isotopic and lithological records from Contessa Highway section in Italy also indicate power dominated by obliquity and eccentricity and precession in Chron19r around 42 Ma (Jovane et al. 2007). Analysis of hyperthermals near the onset of middle-Eocene cooling also show durations of ~40ky, suggesting carbon ventilation controlled by obliquity pacing of high-latitude stratification/overturn (Sexton et al. 2011).

The dominant orbital patterns observed in records from various locations in the middle Eocene, show a complex response to orbital forcing in this transitional period from the early Paleogene, which lacks power in the obliquity bands, to the late Eocene, which is dominated by obliquity. One possible explanation for the transition of orbital signals over the Eocene epoch is changes in Earth's orbit parameters. When the eccentricity is low, the obliquity signals become relatively pronounced without enhancing the absolute values of obliquity. Orbital solutions of Laskar 2004, however, do not predict low eccentricity patterns over this period, though estimates for orbital solutions earlier than 40 Ma could be inaccurate (Laskar et al., 2004, Westerhold et al., 2007). In the lithological records of this study, the wavelength of cycles is reduced in Interval III which reflects the power shifts from a mixture of obliquity and eccentricity signals to obliquity dominance during Interval III, or the sedimentation rate is lower in Interval III than in Intervals I and II. Recent

astronomical calibration from bulk $\delta^{13}C$ records suggest low amplitude of eccentricity signal during the lower and middle part of Chron20r (Westerhold et al., 2015), which is consistent with the weak eccentricity and pronounced obliquity signals observed in site 1408, at least for the main portion of C20R.

The Site 1408 record also has bearing on a related hypothesis regarding changes in Earth's tilt. A reduction in Earth's tilt axis has been proposed to explain the reduced seasonality and latitudinal temperature gradient in the early Paleogene, as well as the lack of a pronounced obliquity signal (e.g. Barron 1984, Sewall and Sloan, 2004). Here I show strong obliquity signals in the middle Eocene site, which combined with the absence of a strong obliquity response in low-latitude regions, suggest that the mid-Eocene was a time of normal tilt, and the stable orbital signals over this 2.5-myr interval indicates absence of variation beyond the normal tilt range.

The covariance and phasing of oscillations between $\delta^{18}O$ and $\delta^{13}C$ and lithological record at Site 1408 provides additional insight into the nature of the climate variability, particularly on the regional scale. The $\delta^{13}C$ reflects on global and/or local variations in the carbon chemistry of seawater, whereas Ca/Fe records of pelagic sediments reflect primarily the ratio of $CaCO_3$ to clay, and thus can be used to infer changes in the flux of either component, and/or variations in the local CCD/lysocline. In the lower section of site 1408, peaks in $\delta^{18}O$ are tightly correlated

with peaks in $\delta^{13}C$ and lows in Ca/Fe in periods of 100-kyr eccentricity and 41-kyr obliquity. The coherencies for $\delta^{18}O$-$\delta^{13}C$ and $\delta^{18}O$-log(Ca/Fe) are over the 95% confidence level in both frequencies (Figure 11). Phase relationship analysis suggests that $\delta^{18}O$ leads log(Ca/Fe) and $\delta^{13}C$ for the 100-kyr period, while the phase lag for the 41-kyr period is less clear. The results suggest that variations in the intensity and distribution of insolation drives changes in both global and regional climate, which in turn leads the response of the global or local carbon cycle, regional climate, circulation and/or deep sea chemistry. The spectral analysis for the upper section (Interval III) lacks power in the specific periods, and thus the coherencies are not sufficiently high to assess phase correlations (Figure 12) a likely artifact of error in the age model. While most of the peaks/lows of these proxies (particularly O and C isotopes) of this interval can be visually correlated (Figure 7), the weak coherencies might result from the high noise to signal ratio, continuous changes in sedimentation rate or a gradual mixture of obliquity and eccentricity power, as such artifacts could dilute the power concentrated in the orbital bands, and produce several weaker peaks in nearby periods, as is observed in Figure 12.

Figure 11. Cross spectrum, coherency, and phase of the $\delta^{18}O$-$\delta^{13}C$ (panels a, c) and $\delta^{18}O$-log(Ca/Fe) (panels b, d) by cross-spectral analysis using Arand program for samples in Interval I based on depth. The detrended samples were resampled with a constant step of 0.0925m, and the number of input samples were 311 in this analysis. Periods of power are converted from depth using average sedimentation rate of 2.8 cm/kyr. The number of lags were set to 100 with a 95% confidence level. Periods representing 100-kyr eccentricity, 41-kyr obliquity and 21-kyr precession are marked in the figure. Both $\delta^{18}O$-$\delta^{13}C$ and $\delta^{18}O$-log(Ca/Fe) are highly coherent in frequencies representing 100-kyr eccentricity and obliquity. The phase correlations are shown only in frequencies representing eccentricity and obliquity with high coherency. The $\delta^{18}O$ signal is indicated to lead $\delta^{13}C$ and Ca/Fe in the 100-kyr period, while the phase lags for the 41-kyr band are weaker.

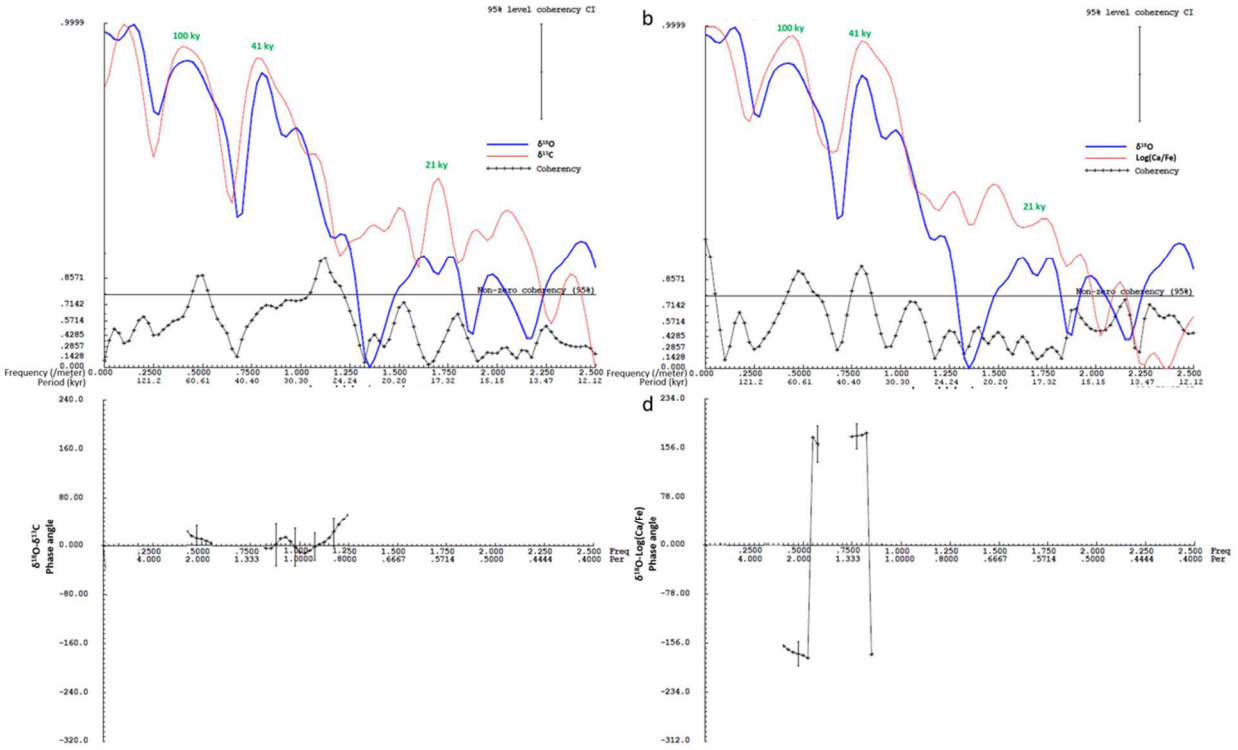
95% level coherency CI
100 ky
41 ky
21 ky
δ18O
δ13C
Coherency
Non-zero coherency (95%)
Frequency (/meter)
Period (kyr)
δ18O-δ13C
Phase angle
b
95% level coherency CI
100 ky
41 ky
21 ky
δ18O
Log(Ca/Fe)
Coherency
Non-zero coherency (95%)
Frequency (/meter)
Period (kyr)
d
δ18O-Log(Ca/Fe)
Phase angle

Figure 12. Cross spectrum and coherency of the $\delta^{18}O$-$\delta^{13}C$ (panel a) and $\delta^{18}O$-log(Ca/Fe) (panel b) by cross-spectral analysis for samples in Interval III using the same approach as shown in Figure 11. The number of resampled input samples is 350 for this interval. Clear peaks in obliquity and eccentricity bands are not observed from the spectrums, and no strong coherencies are shown between the proxies.

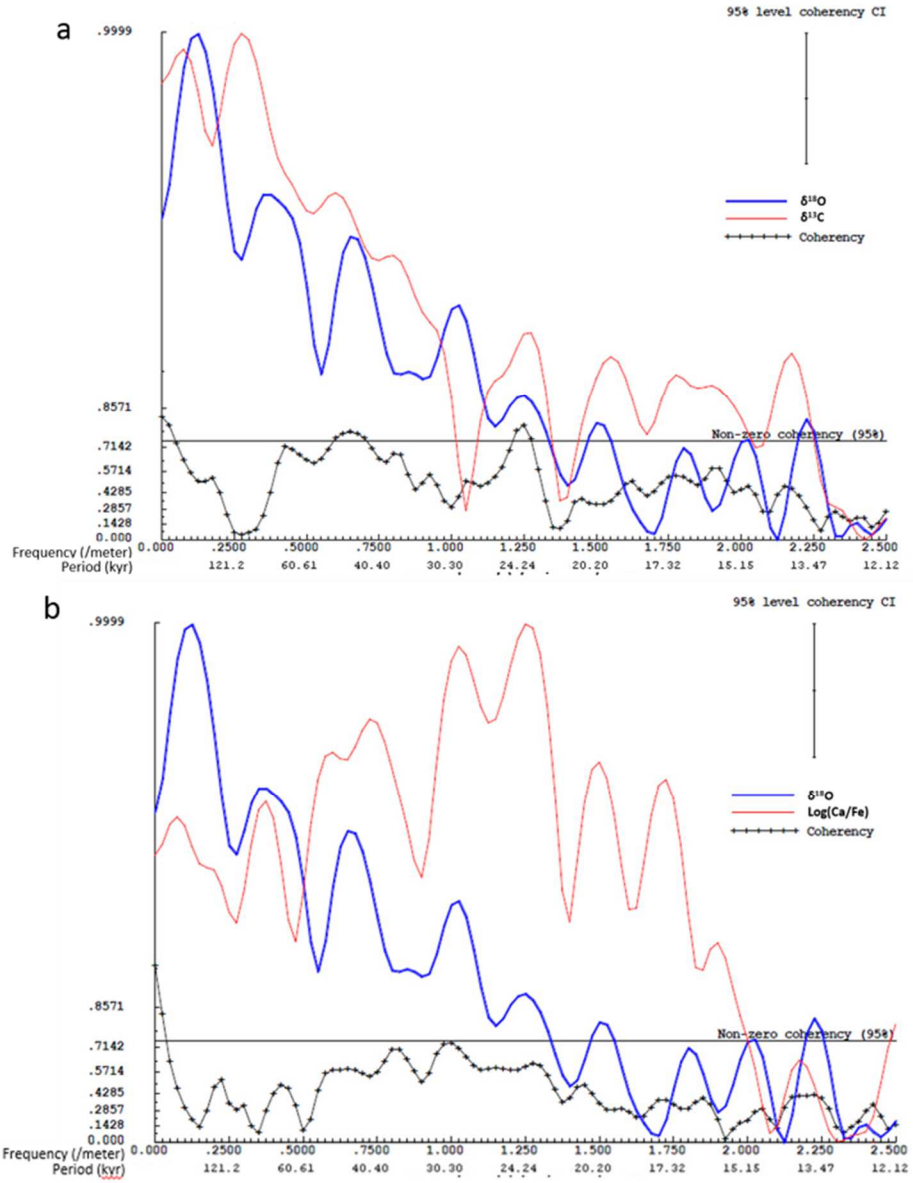
a
95% level coherency CI
.9999
δ18O
δ13C
Coherency
.8571
.7142
.5714
.4285
.2857
.1428
0.000
Non-zero coherency (95%)
Frequency (/meter)
Period (kyr)
0.000
.2500
.5000
.7500
1.000
1.250
1.500
1.750
2.000
2.250
2.500
121.2
60.61
40.40
30.30
24.24
20.20
17.32
15.15
13.47
12.12
b
95% level coherency CI
.9999
δ18O
Log(Ca/Fe)
Coherency
.8571
.7142
.5714
.4285
.2857
.1428
0.000
Non-zero coherency (95%)
Frequency (/meter)
Period (kyr)
0.000
.2500
.5000
.7500
1.000
1.250
1.500
1.750
2.000
2.250
2.500
121.2
60.61
40.40
30.30
24.24
20.20
17.32
15.15
13.47
12.12

The relative phasing in Interval I suggests that the $\delta^{18}O$ leads both $\delta^{13}C$ and Ca/Fe. While an increase of local DIC $\delta^{13}C$ in cooler climate may be caused by decreased metabolism of bacteria which decompose less organic carbon into DIC, the mechanism for the way of coupling between Ca/Fe and stable isotopes in Interval I remains unknown. There are several possibilities, which I briefly explore. Firstly, climatic variations can result in changes in export productivity, as enhanced vertical mixing in cooler climate increases nutrient availability, producing more carbonate/silicate materials which dilute the clay fraction and enhance Ca/Fe ratio (e.g., Norris et al. 2013). However, this process produces reversed Ca/Fe- $\delta^{18}O$ coupled to my observation. Besides, the relatively constant wavelengths between peaks and lows of the lithological records in Interval I suggest stable mass accumulation rates, which also precludes the possibility of a major shift in export productivity.

Second, the most direct coupling between carbon system and climate is associated with precipitation. Riverine erosion and transport contribute terrestrial material into the ocean reservoir. Generally, global precipitation is enhanced in warmer climate, which results in higher clay fraction in pelagic sediments (Schmitz and Pujalte, 2007). However, Ca/Fe minima coincide with peaks in $\delta^{18}O$, which is counter to this hypothesis.

Third, the increased clay fraction linked to cooler climate may be attributed to local ice sheets and/or wind intensity. As discussed above, I don't believe that ice-sheets existed based on Mg/Ca- $\delta^{18}O$ records, through the possibility of small alpine glaciers on Greenland is possible (Eldrett et al. 2007). Ice-rafted debris were also not observed in my section. Therefore, this hypothesis is not supported by existent evidence.

Finally, this relationship could be attributed to changes in bottom water circulation. For example, bottom current could be enhanced when increased latitudinal temperature gradient produced stronger wind-driven ocean circulation in cooler episodes (Bice and Marotzke, 2001). The relationship between $\delta^{18}O$ and $\delta^{13}C$ would be consistent with this mechanism, but not the Fe/Ca.

The coherency between Ca/Fe, $\delta^{13}C$ and $\delta^{18}O$ records weakens in Interval III, and spectral analysis suggests that the major frequency of power in Ca/Fe is higher than that in stable isotope records (Figure 12). The decoupling between Ca/Fe and stable isotope records indicates a potential change in the dominant processes driving the Ca and Fe accumulation. The stable isotope data more likely reflect global signals, whereas variations of lithological records are controlled by local climatic forcing which dominate the cyclic variations of clay flux, so it is possible that a regional shift in climate was responsible for increasing amplitude of the lithologic

cycles. Testing of this idea requires planktonic stable isotope data which records the response of surface ocean to local climate variations.

4.3 Eocene bottom water and N. Atlantic circulation

In general, simulations of Eocene climate and ocean circulation using various coupled ocean atmosphere models (e.g., Huber and Sloan, 2001; Lunt et al., 2010) have produced mixed results for the MOC. In some simulations under "greenhouse" conditions, the MOC is relatively weak with little to no northern component water (Bice and Marotzke, 2001) whereas in other studies, overturning does occur (Lunt et al., 2009). The conflicting results are likely an artifact of imposed boundary conditions, and/or differences in model construct/sensitivity. Regardless, Inter and intra-basin carbon isotope and oxygen isotope gradients can be used to assess whether a MOC similar to modern was present during the Eocene. In a previous study, an increase in the interbasin $\delta^{13}C$ gradient was observed at the end of the early Eocene based on records from Sites 1258 and 1260 in Demerara Rise (Sexton et al. 2006) and the global compilation of Zachos et al. (2001), a shift that was synchronous with the transition from the Early Eocene climatic optimum to the middle-Eocene cooling. This was attributed to one or a combination of factors, the first being a transition from multiple deep water source to a single dominant source in the Southern Ocean. Additionally, or alternatively, increased export productivity

due to enhanced biological pump with increased vertical mixing in a cooler ocean could lower bottom water $\delta^{13}C$, at least locally. Reconciling the contributions of circulation changes on the interbasin $\delta^{13}C$ gradients in the middle Eocene, however, was not possible given the limited spatial and temporal resolution of data, particularly by the lack of, direct $\delta^{13}C$ data from the northern Atlantic (Sexton et al. 2006).

The benthic isotopic records from Site 1408 can be used to constrain the presence or absence of a major source of northern component water in the middle Eocene as the site is located under the typical flow path of Northern sourced water in the Atlantic. Here, I compare the C and O isotope data from site 1408 with available data from sites in the Atlantic, for example, Site 1258, and other sites in the global compilation (Figure 13). As different values of carbon isotope fractionation exist among different species of foraminifera, all the data from *Cibicidoides* are normalized to *N. truempyi* using the offset (*C. eoceanus – N. truempyi* = +0.40‰) and (*Cibicidoides spp.–N. truempyi* = +0.34‰) (Sexton et al. 2006, Katz et al. 2003). The interspecies $\delta^{18}O$ offsets for *Cibcidoides* and *N. truempyi* are negligible, thus no correction is applied to the $\delta^{18}O$ data. Corrections for the disequilibrium fractionations of $\delta^{18}O$ versus seawater are applied to remove the error in calculating seawater temperature using the benthic $\delta^{18}O$ records. The offset used for *N. truempyi* is +0.35‰, and +0.28‰ for *Cibicidoides.* (Katz et al. 2003). Deepwater temperature is calculated using the equation from Bemis et al. (1998):

$$T(^0C) = 16.5(\pm 0.2) - 4.80(\pm 0.16) \times (\delta_c - \delta_{sw})$$

Based on the absence of direct physical evidence for Eocene ice-sheets, I assume the δ_{sw} value is that of ice-free ocean (-1.27‰) for this study.

The interbasin $\delta^{13}C$ reconstruction for the interval between 47 Ma and 43 Ma, though not constrained in detail, is characterized by clear offsets among sites. Data from the northern Atlantic (Site 1408) exhibit low $\delta^{13}C$ values, and there is no significant offset compared with data from equatorial Atlantic (Site 1258) and equatorial Pacific (Site 865). Comparatively, $\delta^{13}C$ values from the southern hemisphere (Site 689, 690 and 748 in the Southern Ocean, Site 527 in the southern Atlantic) are significantly higher. This is consistent with relatively aged bottom water in the north Atlantic, suggesting the water flowing over this site originated not in the northern Atlantic, but elsewhere during the early middle Eocene interval. Interbasin $\delta^{18}O$ reconstructions indicate deep water temperatures of 8-10^{o}C at site 1408 which is within the mid-range of observations globally. As such, this leaves open the possibility of southern sourced waters entering the north Atlantic from the south Atlantic and the Pacific. However, bathymetric reconstructions for the early Eocene suggest that the connections between North Atlantic and Pacific/South Atlantic were not deep (<2 km). Alternatively, the existence of warm saline bottom water (WSBW) from subtropical regions has been posited for the PETM and early Eocene. More recent model simulations of ocean circulation for the early Eocene suggest penetration of warm saline water to mid-depths (between 1475 and 2326 m) from

the western northern Atlantic near the location of site 1408 (CCSM3; Huber, Pers. Comm.). As the paleodepth of site 1408 is ~2600m in the early middle Eocene, it is possible that some of this salty water mixed with colder water to produce a more dense water mass reaching this location. This, along with the partially restricted configuration of the north Atlantic, might have increased stratification slowing the overturning with the basin, thus contributing to the lower $\delta^{13}C$.

Other evidence for the state of carbonate chemistry of bottom water comes from Site 1408 B/Ca records, which is a proxy of deep water carbonate saturation state (Brown et al., 2011). As a water mass migrates, respired CO_2 accumulates by continuous remineralization process, lower [CO_3^{2-}] and producing more corrosive water. Therefore, young water should be more basic with higher carbonate concentration. As this influences the borate concentration, the B/Ca ratio of benthic forams, such as *N. truempyi*, tends to covary with [CO_3]. At site 1408, the *N. truempyi* B/Ca data suggest uniform [CO_3^{2-}] values throughout this interval which were on average significantly lower than modern north Atlantic values, consistent with relatively aged bottom water. Therefore, while I cannot fully constrain global circulation changes, I can conclude that north Atlantic deep water was characterized by low $\delta^{13}C$ and [CO_3^{2-}], precluding the existence of a North Atlantic deep water component, at least similar to modern during the early middle Eocene.

.

Figure 13. Multi-site deep sea (benthic) (a) $\delta^{13}C$ and (b) $\delta^{18}O$ reconstruction for the time interval from 47 Ma to 43 Ma. Red lines represent Site 1408 from this study, processed using 5-point smoothing. Black dots are data from site 1258, equatorial Atlantic (Sexton et al., 2006). All other data are from global compilation of Zachos et al.(2008), including data from equatorial Pacific site 865, southern Atlantic site 527, as well as Southern Ocean sites 689, 690 and 748. Panel c exhibits the location of these sites on the paleo-map of 45 Ma reconstructed by Ocean Drilling Stratigraphic Network Plate Tectonic Reconstruction Service. The $\delta^{13}C$ records from site 1408 and two equatorial sites (1258 and 865) are located at the lower end of the global compilation. The $\delta^{18}O$ values of site 1408 are intermediate within the global compilation.

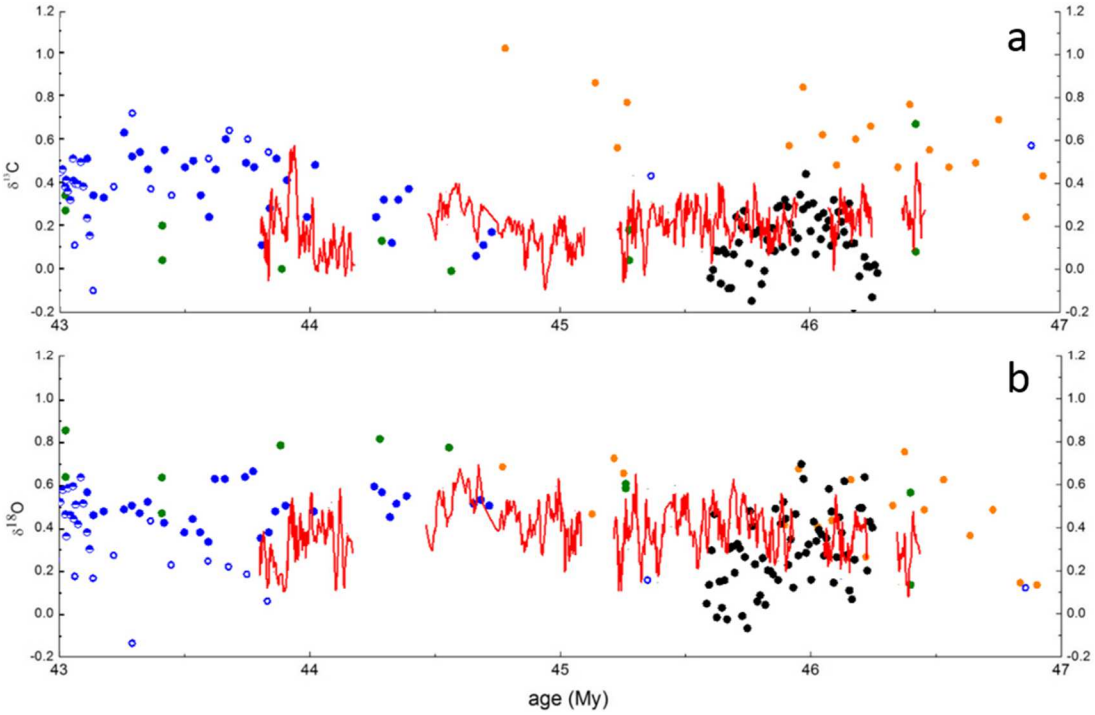

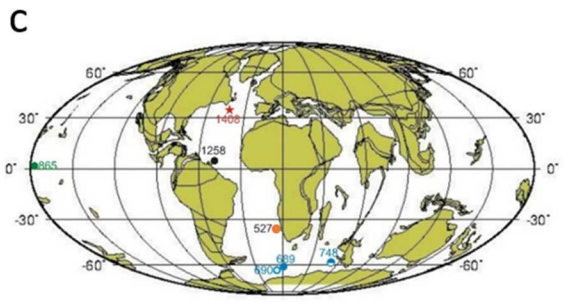

45.0 Ma Reconstruction

Conclusions

I have established the first orbital-resolution stable isotope record for Chron 20r, a ~2.4 my interval, of the early mid-Eocene using sediments from site 1408 in western North Atlantic. These records provide the first insight into several previously poorly understood feature of the paleoceanography of the middle Eocene, including the scale and timing of cooling, orbital scale variations, atmospheric pCO_2 level, sea ice and global circulation. The benthic oxygen isotope records show in detail climate variations during the initial cooling phase from the greenhouse to ice-house world. In particular, I find a gradual cooling trend that is dominated by variability in the obliquity band. Coupled with Mg/Ca data, I estimate nearly constant $\delta^{18}O_{sw}$ in the lower and middle part of this section, indicating no variations in ice volume or the absence of ice sheets. However, a paradox between decreased $\delta^{18}O$ and decreased Mg/Ca ratio is observed in the upper part of this section, which may be induced by a shift in local bottom water $\delta^{18}O$, a hypothesis that can be tested with records from other locations. Comparisons of the site 1408 isotope data with other date from other sites indicate aged water mass flowing over this location, suggesting that the meridional circulation was northward originated from the Southern Ocean, and North Atlantic Deep Water was not initiated in the early middle Eocene.

References

Backman, J., K. Moran, and D. McInroy. "IODP Expedition 302, Arctic Coring Expedition (ACEX): A first look at the Cenozoic paleoceanography of the central Arctic Ocean." *Scientific Drilling* 1 (2005): 12-17.

Barker, S., M. Greaves, and Henry Elderfield. "A study of cleaning procedures used for foraminiferal Mg/Ca paleothermometry." *Geochemistry, Geophysics, Geosystems* 4.9 (2003).

Barron, E. J., and W. M. Washington. "The role of geographic variables in explaining paleoclimates: Results from Cretaceous climate model sensitivity studies." *Journal of Geophysical Research: Atmospheres (1984–2012)* 89.D1 (1984): 1267-1279.

Bemis, E. B., et al. "Reevaluation of the oxygen isotopic composition of planktonic foraminifera: Experimental results and revised paleotemperature equations." *Paleoceanography* 13.2 (1998): 150-160.

Bice, K. L., and J. Marotzke. "Numerical evidence against reversed thermohaline circulation in the warm Paleocene/Eocene ocean." *Journal of Geophysical Research: Oceans (1978–2012)* 106.C6 (2001): 11529-11542.

Bohaty, S. M., and J. C. Zachos. "Significant Southern Ocean warming event in the late middle Eocene." *Geology* 31.11 (2003): 1017-1020.

Bohaty, S. M., et al. "Coupled greenhouse warming and deep-sea acidification in the middle Eocene." *Paleoceanography* 24.2 (2009).

Bohaty, S. M., J. C. Zachos, and M. L. Delaney. "Foraminiferal Mg/Ca evidence for Southern Ocean cooling across the Eocene–Oligocene transition." *Earth and Planetary Science Letters* 317 (2012): 251-261.

Brown, R. E., et al. "A core-top calibration of B/Ca in the benthic foraminifers Nuttallides umbonifera and Oridorsalis umbonatus: A proxy for Cenozoic bottom water carbonate saturation." *Earth and Planetary Science Letters* 310.3 (2011): 360-368.

Cande, S. C., and D. V. Kent. "Revised calibration of the geomagnetic polarity timescale for the Late Cretaceous and Cenozoic." *Journal of geophysical research* 100.B4 (1995): 6093-6095.

Cantalejo, B., and K. T. Pickering. "Orbital forcing as principal driver for fine-grained deep-marine siliciclastic sedimentation, Middle-Eocene Ainsa Basin, Spanish Pyrenees." *Palaeogeography, Palaeoclimatology, Palaeoecology* 421 (2015): 24-47.

Coggon, R. M., et al. "Reconstructing past seawater Mg/Ca and Sr/Ca from mid-ocean ridge flank calcium carbonate veins." *Science* 327.5969 (2010): 1114-1117.

Coxall, H. K., et al. "Rapid stepwise onset of Antarctic glaciation and deeper calcite compensation in the Pacific Ocean." *Nature* 433.7021 (2005): 53-57.

Cramer, B. S., et al. "Late Cretaceous–Neogene trends in deep ocean temperature and continental ice volume: reconciling records of benthic foraminiferal geochemistry (δ18O and

Mg/Ca) with sea level history." *Journal of Geophysical Research: Oceans (1978–2012)* 116.C12 (2011).

Curry, W. B., and D. W. Oppo. "Glacial water mass geometry and the distribution of δ13C of ΣCO2 in the western Atlantic Ocean." *Paleoceanography*20.1 (2005).

Darby, D. A. "Ephemeral formation of perennial sea ice in the Arctic Ocean during the middle Eocene." *Nature Geoscience* 7.3 (2014): 210-213.

DeConto, R. M., et al. "Thresholds for Cenozoic bipolar glaciation." *Nature*455.7213 (2008): 652-656.

de Villiers, S., and B. K. Nelson. "Detection of low-temperature hydrothermal fluxes by seawater Mg and Ca anomalies." *Science* 285.5428 (1999): 721-723.

Dickens, G. R., M. M. Castillo, and J. CG Walker. "A blast of gas in the latest Paleocene: Simulating first-order effects of massive dissociation of oceanic methane hydrate." *Geology* 25.3 (1997): 259-262.

Edgar, K. M., et al. "No extreme bipolar glaciation during the main Eocene calcite compensation shift." *Nature* 448.7156 (2007): 908-911.

Eldrett, J. S., et al. "Continental ice in Greenland during the Eocene and Oligocene." *Nature* 446.7132 (2007): 176-179.

Farkaš, J., et al. "Evolution of the oceanic calcium cycle during the late Mesozoic: evidence from δ 44/40 Ca of marine skeletal carbonates." *Earth and Planetary Science Letters* 253.1 (2007): 96-111.

Galeotti, S., et al. "Orbital chronology of Early Eocene hyperthermals from the Contessa Road section, central Italy." *Earth and Planetary Science Letters*290.1 (2010): 192-200.

Hohbein, M. W., P. F. Sexton, and J. A. Cartwright. "Onset of North Atlantic Deep Water production coincident with inception of the Cenozoic global cooling trend." *Geology* 40.3 (2012): 255-258.

Howell, P. 2001. ARAND time series and spectral analysis package for the Macintosh, Brown University. IGBP PAGES/World Data Center for Paleoclimatology Data Contribution Series #2001-031. NOAA/NGDC
Paleoclimatology Program, Boulder

Huber, M., and L. C. Sloan. "Heat transport, deep waters, and thermal gradients: Coupled simulation of an Eocene greenhouse climate."*Geophys. Res. Lett* 28.18 (2001): 3481-3484.

Huber, M., et al. "Eocene circulation of the Southern Ocean: Was Antarctica kept warm by subtropical waters?." *Paleoceanography* 19.4 (2004).

Huber, M., and D. Nof. "The ocean circulation in the southern hemisphere and its climatic impacts in the Eocene." *Palaeogeography, Palaeoclimatology, Palaeoecology* 231.1 (2006): 9-28.

Jovane, L., et al. "The middle Eocene climatic optimum event in the Contessa Highway section, Umbrian Apennines, Italy." *Geological Society of America Bulletin* 119.3-4 (2007): 413-427.

Katz, M. E., et al. "Early Cenozoic benthic foraminiferal isotopes: Species reliability and interspecies correction factors." *Paleoceanography* 18.2 (2003).

Laskar, J., et al. "A long-term numerical solution for the insolation quantities of the Earth." *Astronomy & Astrophysics* 428.1 (2004): 261-285.

Lear, C. H., H. Elderfield, and P. A. Wilson. "Cenozoic deep-sea temperatures and global ice volumes from Mg/Ca in benthic foraminiferal calcite." *science* 287.5451 (2000): 269-272.

Lear, C. H., Y. Rosenthal, and N. Slowey. "Benthic foraminiferal Mg/Ca-paleothermometry: A revised core-top calibration." *Geochimica et Cosmochimica Acta* 66.19 (2002): 3375-3387.

Littler, K., et al. "A high-resolution benthic stable-isotope record for the South Atlantic: Implications for orbital-scale changes in Late Paleocene–Early Eocene climate and carbon cycling." *Earth and Planetary Science Letters* 401 (2014): 18-30.

Lourens, L. J., et al. "Astronomical pacing of late Palaeocene to early Eocene global warming events." *Nature* 435.7045 (2005): 1083-1087.

Lunt, D. J., et al. "CO2-driven ocean circulation changes as an amplifier of Paleocene-Eocene thermal maximum hydrate destabilization." *Geology* 38.10 (2010): 875-878.

Mewes, A., et al. "Impact of seawater Ca2+ on the calcification and calcite Mg/Ca of Amphistegina lessonii." *Biogeosciences Discussions* 11 (2014): 17463-17489.

Miller, K. G., J. D. Wright, and Richard G. Fairbanks. "Unlocking the ice house: Oligocene-Miocene oxygen isotopes, eustasy, and margin erosion."*Journal of Geophysical Research: Solid Earth (1978–2012)* 96.B4 (1991): 6829-6848.

Miller, K. G. "Southern Ocean influences on late Eocene to Miocene deepwater circulation." *The Antarctic paleoenvironment: a perspective on global change* 60 (1993): 1-25.

Miller, K. G., et al. "The Phanerozoic record of global sea-level change."*science* 310.5752 (2005): 1293-1298.

Miller, K. G., et al. "A view of Antarctic ice-sheet evolution from sea-level and deep-sea isotope changes during the Late Cretaceous–Cenozoic." *Antarctica: a keystone in a changing world* (2008): 55-70.

Norris, R. D., A. Klaus, and D. Kroon. "Mid-Eocene deep water, the late Palaeocene thermal maximum and continental slope mass wasting during the Cretaceous-Palaeogene impact." *Geological Society, London, Special Publications* 183.1 (2001): 23-48.

Norris, R. D., et al. "Marine ecosystem responses to Cenozoic global change."*Science* 341.6145 (2013): 492-498.

Pagani, M., et al. "Marked decline in atmospheric carbon dioxide concentrations during the Paleogene." *Science* 309.5734 (2005): 600-603.

Pälike, Heiko, et al. "The heartbeat of the Oligocene climate system." *science*314.5807 (2006): 1894-1898.

Pearson, P. N., G. L. Foster, and B. S. Wade. "Atmospheric carbon dioxide through the Eocene–Oligocene climate transition." *Nature* 461.7267 (2009): 1110-1113.

Roemmich, D., and J. Gilson. "The 2004–2008 mean and annual cycle of temperature, salinity, and steric height in the global ocean from the Argo Program." *Progress in Oceanography* 82.2 (2009): 81-100.

Rosenthal, Y., E. A. Boyle, and N. Slowey. "Temperature control on the incorporation of magnesium, strontium, fluorine, and cadmium into benthic foraminiferal shells from Little Bahama Bank: Prospects for thermocline paleoceanography." *Geochimica et Cosmochimica Acta* 61.17 (1997): 3633-3643.

Rosenthal, Y., et al. "Temperature and carbonate ion effects on Mg/Ca and Sr/Ca ratios in benthic foraminifera: Aragonitic species Hoeglundina elegans."*Paleoceanography* 21.1 (2006).

Scher, H. D., and E. E. Martin. "Timing and climatic consequences of the opening of Drake Passage." *Science* 312.5772 (2006): 428-430.

Schmitz, B., and V. Pujalte. "Abrupt increase in seasonal extreme precipitation at the Paleocene-Eocene boundary." *Geology* 35.3 (2007): 215-218.

Segev, E., and J. Erez. "Effect of Mg/Ca ratio in seawater on shell composition in shallow benthic foraminifera." *Geochemistry, Geophysics, Geosystems* 7.2 (2006).

Sewall, J. O., and L. C. Sloan. "Less ice, less tilt, less chill: The influence of a seasonally ice-free Arctic Ocean and reduced obliquity on early Paleogene climate." *Geology* 32.6 (2004): 477-480.

Sexton, P. F., P. A. Wilson, and R. D. Norris. "Testing the Cenozoic multisite composite δ18O and δ13C curves: New monospecific Eocene records from a single locality, Demerara Rise (Ocean Drilling Program Leg 207)."*Paleoceanography* 21.2 (2006).

Sexton, P. F., et al. "Eocene global warming events driven by ventilation of oceanic dissolved organic carbon." *Nature* 471.7338 (2011): 349-352.

Stickley, C. E., et al. "Evidence for middle Eocene Arctic sea ice from diatoms and ice-rafted debris." *Nature* 460.7253 (2009): 376-379.

Westerhold, Thomas, et al. "On the duration of magnetochrons C24r and C25n and the timing of early Eocene global warming events: Implications from the Ocean Drilling Program Leg 208 Walvis Ridge depth transect."*Paleoceanography* 22.2 (2007).

Westerhold, T., and U. Röhl. "High resolution cyclostratigraphy of the early Eocene–new insights into the origin of the Cenozoic cooling trend." *Climate of the Past* 5.3 (2009): 309-327.

Westerhold, Thomas, and U. Röhl. "Orbital pacing of Eocene climate during the Middle Eocene Climate Optimum and the chron C19r event: Missing link found in the tropical western Atlantic." *Geochemistry, Geophysics, Geosystems* 14.11 (2013): 4811-4825.

Westerhold, T., et al. "Astronomical calibration of the geological timescale: closing the middle Eocene gap." *Climate of the Past Discussions* 11.3 (2015).

Via, R. K., and D. J. Thomas. "Evolution of Atlantic thermohaline circulation: Early Oligocene onset of deep-water production in the North Atlantic." *Geology* 34.6 (2006): 441-444.

Zachos, J. C., et al. "Trends, rhythms, and aberrations in global climate 65 Ma to present." *Science* 292.5517 (2001): 686-693.

Zachos, J. C., G. R. Dickens, and R. E. Zeebe. "An early Cenozoic perspective on greenhouse warming and carbon-cycle dynamics."*Nature* 451.7176 (2008): 279-283.

Zachos, J. C., et al. "Tempo and scale of late Paleocene and early Eocene carbon isotope cycles: Implications for the origin of hyperthermals."*Earth and Planetary Science Letters* 299.1 (2010): 242-249.

Zeebe, R. E., J. C. Zachos, and G. R. Dickens. "Carbon dioxide forcing alone insufficient to explain Palaeocene–Eocene Thermal Maximum warming." *Nature Geoscience* 2.8 (2009): 576-580.

Appendix

TABLE 1. Benthic foraminiferal stable isotope records for site 1408

HOLE	CORE	SECTION	TOP_DEPTH	BOTTOM_DEPTH	MCD (m)	$\delta^{13}C$	$\delta^{18}O$
B	19	1	25	27	166.03	0.15	-0.13
B	19	1	31	33	166.09	0.24	-0.16
B	19	1	37	39	166.15	0.28	0.08
B	19	1	43	45	166.21	0.14	-0.05
B	19	1	49	51	166.27	0.18	-0.10
B	19	1	55	57	166.33	0.20	-0.01
B	19	1	61	63	166.39	0.23	0.03
B	19	1	67	69	166.45	0.06	-0.01
B	19	1	73	75	166.51	0.25	0.06
B	19	1	79	81	166.57	-0.11	0.02
B	19	1	91	93	166.69	0.09	-0.07
B	19	1	97	99	166.75	0.17	-0.10
B	19	1	103	105	166.81	0.12	-0.05
B	19	1	109	111	166.87	-0.02	-0.18
B	19	1	115	117	166.93	0.04	-0.26
B	19	1	121	123	166.99	-0.14	-0.17
B	19	1	127	129	167.05	0.08	-0.22
B	19	1	133	135	167.11	0.22	-0.16
B	19	1	139	141	167.17	0.27	-0.17
B	19	2	1	3	167.29	0.40	0.03
B	19	2	7	9	167.35	0.33	-0.07
B	19	2	13	15	167.41	0.21	-0.11
B	19	2	25	27	167.53	0.18	0.02
B	19	2	31	33	167.59	0.15	-0.10
B	19	2	37	39	167.65	0.24	-0.09
B	19	2	43	45	167.71	0.30	-0.15
B	19	2	49	51	167.77	0.32	-0.10
B	19	2	55	57	167.83	0.34	-0.09
B	19	2	61	63	167.89	0.24	-0.18
B	19	2	79	81	168.07	0.30	-0.20
B	19	2	83	85	168.11	0.23	-0.20
B	19	2	87	89	168.15	0.30	-0.12
B	19	2	93	95	168.21	0.19	-0.20
B	19	2	99	101	168.27	0.16	-0.15
B	19	2	111	113	168.39	0.18	-0.14
B	19	2	117	119	168.45	0.16	-0.22
B	19	2	123	125	168.51	0.19	-0.21
B	19	2	129	131	168.57	0.20	-0.27
B	19	2	135	137	168.63	0.06	-0.22
B	19	2	141	143	168.69	0.20	-0.23

B	19	2	147	149	168.75	0.29	-0.26
B	19	3	1	3	168.79	0.13	-0.18
B	19	3	7	9	168.85	0.20	-0.22
B	19	3	13	15	168.91	0.30	-0.10
B	19	3	19	21	168.97	0.38	-0.15
B	19	3	25	27	169.03	0.44	-0.06
B	19	3	31	33	169.09	0.45	0.05
B	19	3	37	39	169.15	0.53	0.11
B	19	3	43	45	169.21	0.55	0.08
B	19	3	49	51	169.27	0.45	0.13
B	19	3	55	57	169.33	0.48	0.17
B	19	3	61	63	169.39	0.53	0.16
B	19	3	67	69	169.45	0.53	-0.01
B	19	3	73	75	169.51	0.55	0.19
B	19	3	79	81	169.57	0.57	0.12
B	19	3	85	87	169.63	0.51	0.14
B	19	3	91	93	169.69	0.50	0.08
B	19	3	97	99	169.75	0.43	-0.12
B	19	3	103	105	169.81	0.37	0.02
B	19	3	109	111	169.87	0.30	-0.11
B	19	3	115	117	169.93	0.23	0.07
B	19	3	121	123	169.99	0.24	0.00
B	19	3	127	129	170.05	0.15	-0.04
B	19	3	133	135	170.11	0.03	-0.10
B	19	3	139	141	170.17	0.15	-0.02
B	19	3	145	147	170.23	0.10	0.01
B	19	4	1	3	170.29	0.16	0.08
B	19	4	7	9	170.35	0.12	0.13
B	19	4	13	15	170.41	0.11	0.06
B	19	4	19	21	170.47	0.17	0.08
B	19	4	25	27	170.53	0.29	0.03
B	19	4	31	33	170.59	0.12	-0.17
B	19	4	37	39	170.65	0.12	0.10
B	19	4	43	45	170.71	0.07	0.06
B	19	4	49	51	170.77	0.09	-0.08
B	19	4	55	57	170.83	0.18	0.01
B	19	4	61	63	170.89	0.20	0.06
B	19	4	67	69	170.95	0.18	-0.03
B	19	4	73	75	171.01	0.21	-0.07
B	19	4	79	81	171.07	0.13	-0.07
B	19	4	85	87	171.13	0.15	0.07
B	19	4	97	99	171.25	0.11	0.05
B	19	4	103	105	171.31	0.03	-0.04
B	19	4	109	111	171.37	0.25	0.00
B	19	4	115	117	171.43	0.15	0.10
B	19	4	121	123	171.49	0.18	0.08
B	19	4	127	129	171.55	0.27	0.22
B	19	4	133	135	171.61	0.22	0.12

B	19	4	139	141	171.67	0.35	0.25
B	19	4	145	147	171.73	0.32	0.24
A	17	1	79	81	171.77	0.38	0.09
A	17	1	85	87	171.83	0.41	0.04
A	17	1	91	93	171.89	0.43	0.01
A	17	1	97	99	171.95	0.35	0.03
A	17	1	103	105	172.01	0.26	-0.05
A	17	1	109	111	172.07	0.27	0.06
A	17	1	115	117	172.13	0.33	-0.03
A	17	1	121	123	172.19	0.36	0.02
A	17	1	127	129	172.25	0.46	-0.01
A	17	1	133	135	172.31	0.41	0.06
A	17	1	139	141	172.37	0.37	0.07
A	17	1	145	147	172.43	0.36	0.12
A	17	2	1	3	172.49	0.41	0.02
A	17	2	7	9	172.55	0.29	0.07
A	17	2	13	15	172.61	0.29	0.05
A	17	2	19	21	172.67	0.36	0.01
A	17	2	25	27	172.73	0.35	0.17
A	17	2	31	33	172.79	0.39	0.14
A	17	2	43	45	172.91	0.35	-0.07
A	17	2	49	51	172.97	0.38	0.04
A	17	2	55	57	173.03	0.30	0.00
A	17	2	61	63	173.09	0.31	0.07
A	17	2	67	69	173.15	0.32	-0.03
A	17	2	73	75	173.21	0.31	0.11
A	17	2	79	81	173.27	0.39	0.15
A	17	2	85	87	173.33	0.37	0.10
A	17	2	91	93	173.39	0.28	0.12
A	17	2	97	99	173.45	0.27	-0.05
A	17	2	103	105	173.51	0.25	0.17
A	17	2	109	111	173.57	0.21	0.06
A	17	2	115	117	173.63	0.15	0.12
A	17	2	121	123	173.69	0.12	0.01
A	17	2	127	129	173.75	0.11	-0.06
A	17	2	133	135	173.81	0.05	-0.07
A	17	2	139	141	173.87	0.06	-0.23
A	17	2	145	147	173.93	-0.04	-0.18
A	17	3	7	9	174.05	0.04	-0.23
A	17	3	13	15	174.11	0.09	-0.02
A	17	3	19	21	174.17	0.15	0.00
A	17	3	25	27	174.23	0.05	0.03
A	17	3	31	33	174.29	0.18	0.17
A	17	3	37	39	174.35	0.09	0.30
A	17	3	43	45	174.41	0.17	0.12
A	17	3	49	51	174.47	0.16	0.04
A	17	3	55	57	174.53	0.19	0.01
A	17	3	61	63	174.59	-0.03	-0.07

A	17	3	67	69	174.65	-0.03	-0.25
A	17	3	73	75	174.71	0.02	-0.20
A	17	3	79	81	174.77	-0.04	-0.14
A	17	3	85	87	174.83	0.06	-0.03
A	17	3	91	93	174.89	0.13	-0.11
A	17	3	97	99	174.95	-0.03	0.03
A	17	3	103	105	175.01	0.35	0.02
A	17	3	115	117	175.13	0.06	-0.03
A	17	3	121	123	175.19	0.04	0.02
A	17	3	127	129	175.25	-0.03	0.01
A	17	3	133	135	175.31	0.10	-0.04
A	17	3	139	141	175.37	-0.03	0.02
A	17	3	145	147	175.43	0.03	-0.08
A	17	4	1	3	175.49	0.15	0.13
A	17	4	13	15	175.61	0.21	0.11
A	17	4	19	21	175.67	0.28	0.06
A	17	4	31	33	175.79	0.39	0.25
A	17	4	43	45	175.91	0.38	0.20
A	17	4	55	57	176.03	0.37	0.28
A	17	4	67	69	176.15	0.29	0.27
A	17	4	79	81	176.27	0.30	0.20
A	17	4	91	93	176.39	0.31	0.31
A	17	4	103	105	176.51	0.21	0.11
A	17	4	115	117	176.63	0.20	0.18
A	17	4	127	129	176.75	0.21	0.07
A	17	4	139	141	176.87	0.20	0.20
A	17	4	145	147	176.93	0.14	0.06
A	17	5	1	3	176.99	0.11	0.01
A	17	5	13	15	177.11	-0.04	-0.17
A	17	5	25	27	177.23	-0.06	0.01
A	17	5	37	39	177.35	0.16	0.17
A	17	5	49	51	177.47	0.18	0.09
A	17	5	61	63	177.59	0.02	0.11
A	17	5	73	75	177.71	0.32	0.25
A	17	5	85	87	177.83	0.26	0.20
A	17	5	97	99	177.95	0.32	0.22
A	17	5	103	105	178.01	0.20	0.09
C	19	5	106	108	178.22	0.20	0.22
C	19	5	130	132	178.46	-0.07	-0.02
C	19	6	4	6	178.7	0.03	0.25
C	19	6	28	30	178.94	-0.06	-0.04
C	19	6	40	42	179.06	0.16	0.11
C	19	6	52	54	179.18	0.34	0.14
C	19	6	76	78	179.42	0.10	-0.26
C	19	6	88	90	179.54	0.03	-0.05
B	20	1	43	45	179.57	0.22	0.08
B	20	1	55	57	179.69	0.29	0.22
B	20	1	61	63	179.75	0.22	0.18

B	20	1	73	75	179.87	0.20	0.10
B	20	1	79	81	179.93	0.15	0.16
B	20	1	85	87	179.99	0.21	0.05
B	20	1	97	99	180.11	0.22	0.06
B	20	1	109	111	180.23	0.25	0.11
B	20	1	121	123	180.35	0.33	0.23
B	20	1	127	129	180.41	0.24	-0.31
B	20	1	139	141	180.53	0.26	0.25
B	20	2	1	3	180.65	0.37	0.21
B	20	2	7	9	180.71	0.25	0.17
B	20	2	19	21	180.83	0.30	0.20
B	20	2	31	33	180.95	0.16	0.03
B	20	2	37	39	181.01	0.27	0.13
B	20	2	49	51	181.13	0.11	0.04
B	20	2	55	57	181.19	0.38	0.13
B	20	2	73	75	181.37	0.28	0.20
B	20	2	79	81	181.43	0.35	0.28
B	20	2	97	99	181.61	-0.10	-0.35
B	20	2	103	105	181.67	0.24	-0.07
B	20	2	121	123	181.85	0.30	0.12
B	20	2	133	135	181.97	0.22	0.03
B	20	2	139	141	182.03	0.28	0.03
B	20	3	7	9	182.21	0.16	-0.04
B	20	3	19	21	182.33	0.33	0.15
B	20	3	31	33	182.45	0.37	0.21
B	20	3	43	45	182.57	0.36	0.26
B	20	3	55	57	182.69	0.33	0.19
B	20	3	61	63	182.75	0.34	0.37
B	20	3	67	69	182.81	0.27	0.25
B	20	4	79	81	184.43	0.27	0.06
B	20	4	97	99	184.61	0.22	0.02
B	20	4	109	111	184.73	0.19	0.00
B	20	4	127	129	184.91	0.22	-0.08
B	20	4	139	141	185.03	0.09	-0.01
B	20	4	145	147	185.09	0.17	0.10
C	20	1	91	93	185.11	0.29	-0.02
B	20	5	7	9	185.21	0.19	0.06
C	20	1	103	105	185.23	0.32	0.17
B	20	5	19	21	185.33	0.21	0.15
C	20	1	115	117	185.35	0.35	0.21
C	20	1	121	123	185.41	0.37	0.20
B	20	5	37	39	185.51	0.27	0.24
C	20	1	133	135	185.53	0.26	0.22
B	20	5	43	45	185.57	0.22	0.16
C	20	1	145	147	185.65	0.37	0.23
B	20	5	55	57	185.69	0.23	0.15
C	20	2	7	9	185.77	0.31	0.13
B	20	5	67	69	185.81	0.21	0.24

C	20	2	19	21	185.89	0.36	0.23
B	20	5	79	81	185.93	0.21	0.04
C	20	2	31	33	186.01	0.33	0.19
B	20	5	91	93	186.05	0.20	0.06
C	20	2	43	45	186.13	0.34	0.09
C	20	2	49	51	186.19	0.35	0.08
C	20	2	61	63	186.31	0.33	0.13
C	20	2	73	75	186.43	0.38	0.10
C	20	2	85	87	186.55	0.39	0.13
C	20	2	97	99	186.67	0.33	0.18
C	20	2	103	105	186.73	0.44	0.34
C	20	2	109	111	186.79	0.37	0.21
C	20	2	115	117	186.85	0.31	0.24
C	20	2	121	123	186.91	0.40	0.28
C	20	2	127	129	186.97	0.38	0.26
C	20	2	133	135	187.03	0.35	0.26
C	20	2	139	141	187.09	0.26	0.31
C	20	2	145	147	187.15	0.33	0.30
C	20	3	1	3	187.21	0.23	0.33
C	20	3	13	15	187.33	0.26	0.32
C	20	3	25	27	187.45	0.29	0.20
C	20	3	31	33	187.51	0.33	0.25
C	20	3	37	39	187.57	0.27	0.23
C	20	3	43	45	187.63	0.40	0.29
C	20	3	49	51	187.69	0.23	0.30
C	20	3	55	57	187.75	0.30	0.22
C	20	3	61	63	187.81	0.25	0.21
C	20	3	67	69	187.87	0.20	0.12
C	20	3	73	75	187.93	0.15	0.24
C	20	3	79	81	187.99	0.20	0.12
C	20	3	85	87	188.05	0.16	0.19
C	20	3	91	93	188.11	0.07	0.07
C	20	3	97	99	188.17	0.21	0.19
C	20	3	103	105	188.23	0.24	0.21
C	20	3	109	111	188.29	0.25	0.27
C	20	3	115	117	188.35	0.28	0.35
C	20	3	121	123	188.41	0.33	0.34
C	20	3	127	129	188.47	0.21	0.18
C	20	3	133	135	188.53	0.31	0.36
C	20	3	145	147	188.65	0.32	0.12
B	21	1	49	51	189.41	0.14	0.07
B	21	1	61	63	189.53	0.14	0.07
B	21	1	79	81	189.71	0.16	0.03
B	21	1	85	87	189.77	0.19	0.09
B	21	1	91	93	189.83	0.25	0.05
B	21	1	97	99	189.89	0.19	0.11
B	21	1	103	105	189.95	0.17	0.03
B	21	1	115	117	190.07	0.13	0.03

B	21	1	121	123	190.13	0.17	0.12
B	21	1	133	135	190.25	0.23	0.12
B	21	1	139	141	190.31	0.12	0.12
B	21	1	145	147	190.37	0.29	0.03
B	21	2	13	15	190.55	0.22	0.08
B	21	2	19	21	190.61	0.19	0.27
B	21	2	25	27	190.67	0.23	0.11
B	21	2	31	33	190.73	0.23	0.09
B	21	2	37	39	190.79	0.20	0.21
B	21	2	43	45	190.85	0.11	0.18
B	21	2	49	51	190.91	0.25	0.12
B	21	2	55	57	190.97	0.17	0.14
B	21	2	61	63	191.03	0.23	0.15
B	21	2	67	69	191.09	0.25	0.15
B	21	2	73	75	191.15	0.12	0.18
B	21	2	79	81	191.21	0.16	0.19
B	21	2	85	87	191.27	0.25	0.13
B	21	2	91	93	191.33	0.18	0.12
B	21	2	97	99	191.39	0.22	0.06
B	21	2	103	105	191.45	0.19	0.10
B	21	2	109	111	191.51	0.13	0.12
B	21	2	121	123	191.63	0.19	0.13
B	21	2	127	129	191.69	0.20	0.10
B	21	2	145	147	191.87	0.15	0.00
B	21	3	1	3	191.93	-0.03	-0.02
B	21	3	7	9	191.99	0.07	0.00
B	21	3	13	15	192.05	0.00	0.04
B	21	3	19	21	192.11	-0.04	0.00
B	21	3	25	27	192.17	0.07	-0.03
B	21	3	31	33	192.23	0.04	0.00
B	21	3	37	39	192.29	0.07	-0.01
B	21	3	43	45	192.35	0.16	-0.04
B	21	3	55	57	192.47	-0.02	-0.09
B	21	3	61	63	192.53	0.08	0.02
B	21	3	67	69	192.59	0.19	-0.06
B	21	3	73	75	192.65	0.20	0.01
B	21	3	79	81	192.71	0.09	-0.04
B	21	3	85	87	192.77	0.15	-0.02
B	21	3	91	93	192.83	0.18	-0.01
B	21	3	97	99	192.89	0.17	0.03
B	21	3	103	105	192.95	0.23	0.06
B	21	3	109	111	193.01	0.18	0.02
B	21	3	115	117	193.07	0.18	0.04
B	21	3	121	123	193.13	0.22	0.04
B	21	3	127	129	193.19	0.22	0.12
B	21	3	133	135	193.25	0.22	0.14
B	21	3	139	141	193.31	0.19	0.00
B	21	3	145	147	193.37	0.13	0.07

B	21	4	1	3	193.43	0.14	-0.02
B	21	4	7	9	193.49	0.11	0.03
B	21	4	13	15	193.55	0.12	0.10
B	21	4	25	27	193.67	0.15	0.04
B	21	4	31	33	193.73	0.06	0.02
B	21	4	37	39	193.79	0.08	0.06
B	21	4	49	51	193.91	0.16	0.13
B	21	4	55	57	193.97	0.13	0.06
B	21	4	61	63	194.03	0.12	0.13
A	19	2	115	117	194.03	0.19	-0.04
A	19	2	121	123	194.09	0.17	0.10
B	21	4	67	69	194.09	0.20	0.22
B	21	4	73	75	194.15	0.13	0.15
A	19	2	127	129	194.15	0.33	0.01
B	21	4	79	81	194.21	0.13	0.17
B	21	4	85	87	194.27	0.02	0.16
A	19	2	139	141	194.27	0.10	0.07
A	19	2	145	147	194.33	0.08	0.13
B	21	4	97	99	194.39	-0.04	-0.02
A	19	3	1	3	194.39	0.20	0.23
B	21	4	103	105	194.45	-0.03	-0.11
B	21	4	109	111	194.51	-0.13	0.02
B	21	4	115	117	194.57	-0.06	-0.11
A	19	3	19	21	194.57	0.04	-0.21
B	21	4	121	123	194.63	-0.10	-0.06
A	19	3	25	27	194.63	0.22	0.23
A	19	3	31	33	194.69	0.17	0.08
B	21	4	133	135	194.75	-0.10	-0.01
B	21	4	139	141	194.81	0.00	-0.01
A	19	3	43	45	194.81	0.18	-0.08
A	19	3	49	51	194.87	0.23	0.24
B	21	5	1	3	194.93	-0.02	0.01
A	19	3	55	57	194.93	0.22	0.07
A	19	3	73	75	195.11	0.19	0.07
B	21	5	25	27	195.17	0.01	0.16
A	19	3	79	81	195.17	0.17	0.14
A	19	3	85	87	195.23	0.19	0.00
B	21	5	37	39	195.29	0.07	0.21
A	19	3	91	93	195.29	0.14	0.05
B	21	5	43	45	195.35	0.06	0.18
A	19	3	97	99	195.35	0.14	0.10
A	19	3	103	105	195.41	0.12	-0.07
B	21	5	49	51	195.41	0.15	0.23
B	21	5	55	57	195.47	0.08	0.17
A	19	3	109	111	195.47	0.08	-0.11
A	19	3	115	117	195.53	0.07	-0.17
B	21	5	61	63	195.53	0.10	0.21

B	21	5	67	69	195.59	0.08	0.09
A	19	3	121	123	195.59	0.09	0.03
A	19	3	127	129	195.65	0.16	-0.01
A	19	3	133	135	195.71	0.18	0.04
B	21	5	79	81	195.71	0.19	0.15
A	19	3	139	141	195.77	0.20	0.00
B	21	5	85	87	195.77	0.21	0.09
A	19	3	145	147	195.83	0.15	-0.04
B	21	5	91	93	195.83	0.18	0.18
A	19	4	1	3	195.89	0.07	0.11
B	21	5	97	99	195.89	0.18	0.08
A	19	4	7	9	195.95	0.08	0.08
B	21	5	103	105	195.95	0.11	0.12
A	19	4	13	15	196.01	0.12	0.09
B	21	5	109	111	196.01	0.13	0.07
A	19	4	19	21	196.07	0.15	0.12
B	21	5	115	117	196.07	0.20	0.10
A	19	4	25	27	196.13	0.14	0.12
B	21	5	121	123	196.13	0.23	0.11
A	19	4	31	33	196.19	0.13	0.14
B	21	5	127	129	196.19	0.20	0.15
A	19	4	37	39	196.25	0.15	0.29
B	21	5	133	135	196.25	0.24	0.12
A	19	4	43	45	196.31	0.22	0.25
B	21	5	139	141	196.31	0.24	0.12
A	19	4	49	51	196.37	0.17	0.18
B	21	5	145	147	196.37	0.20	0.09
B	21	6	1	3	196.43	0.19	0.06
A	19	4	55	57	196.43	0.22	0.15
A	19	4	61	63	196.49	0.19	0.17
B	21	6	7	9	196.49	0.28	0.19
A	19	4	67	69	196.55	0.18	0.30
B	21	6	19	21	196.61	0.15	0.17
A	19	4	73	75	196.61	0.16	0.29
A	19	4	79	81	196.67	0.19	0.22
B	21	6	25	27	196.67	0.25	0.17
A	19	4	85	87	196.73	0.14	0.25
B	21	6	31	33	196.73	0.29	0.07
A	19	4	91	93	196.79	0.12	0.24
B	21	6	37	39	196.79	0.24	0.15
A	19	4	97	99	196.85	0.19	-0.03
B	21	6	43	45	196.85	0.29	0.11
A	19	4	103	105	196.91	0.21	0.17
A	19	4	109	111	196.97	0.14	0.09
B	21	6	55	57	196.97	0.24	0.11
A	19	4	115	117	197.03	0.07	0.15
B	21	6	61	63	197.03	0.16	0.06
A	19	4	121	123	197.09	0.07	0.08

B	21	6	67	69	197.09	0.21	0.07
A	19	4	127	129	197.15	0.06	0.09
B	21	6	73	75	197.15	0.12	-0.03
A	19	4	133	135	197.21	-0.03	-0.10
B	21	6	79	81	197.21	0.20	-0.18
A	19	4	139	141	197.27	0.00	-0.08
B	21	6	85	87	197.27	0.13	0.04
A	19	4	145	147	197.33	0.04	0.03
B	21	6	91	93	197.33	0.15	0.05
A	19	5	1	3	197.39	0.06	0.02
B	21	6	97	99	197.39	0.06	0.04
A	19	5	7	9	197.45	0.09	0.02
B	21	6	103	105	197.45	0.14	0.00
B	21	6	109	111	197.51	0.04	0.03
A	19	5	13	15	197.51	0.09	0.07
A	19	5	19	21	197.57	0.01	-0.12
A	19	5	25	27	197.63	0.03	-0.07
B	21	6	121	123	197.63	0.04	-0.06
B	21	6	127	129	197.69	0.09	-0.10
A	19	5	31	33	197.69	0.12	0.01
A	19	5	37	39	197.75	0.11	-0.10
A	19	5	43	45	197.81	0.05	0.07
A	19	5	49	51	197.87	0.03	0.07
B	21	7	1	3	197.93	0.01	-0.01
A	19	5	55	57	197.93	0.11	0.08
B	21	7	7	9	197.99	0.05	-0.10
B	21	7	13	15	198.05	0.06	-0.02
A	19	5	67	69	198.05	0.18	-0.02
A	19	5	73	75	198.11	0.15	0.01
B	21	7	25	27	198.17	0.14	-0.06
A	19	5	79	81	198.17	0.16	0.05
A	19	5	85	87	198.23	0.11	0.13
B	21	7	31	33	198.23	0.18	-0.11
A	19	5	91	93	198.29	0.10	0.03
B	21	7	37	39	198.29	0.13	-0.07
A	19	5	97	99	198.35	0.15	0.12
A	19	5	103	105	198.41	0.11	0.13
A	19	5	109	111	198.47	0.21	0.03
A	19	5	115	117	198.53	0.12	-0.02
A	19	5	127	129	198.65	0.02	0.21
A	19	5	133	135	198.71	0.11	0.11
A	19	5	139	141	198.77	0.13	-0.01
A	19	5	145	147	198.83	0.18	0.02
A	20	1	91	93	202.29	0.14	0.02
A	20	1	103	105	202.41	0.29	0.03
A	20	1	115	117	202.53	0.12	0.20
A	20	1	121	123	202.59	0.16	0.01
A	20	1	127	129	202.65	0.19	0.04

A	20	1	133	135	202.71	0.24	0.00
B	22	2	43	45	202.75	0.02	-0.22
A	20	1	139	141	202.77	0.18	-0.17
B	22	2	49	51	202.81	0.05	-0.24
B	22	2	55	57	202.87	0.05	-0.03
A	20	2	1	3	202.89	-0.09	-0.11
B	22	2	61	63	202.93	-0.03	-0.12
A	20	2	7	9	202.95	-0.03	-0.31
B	22	2	67	69	202.99	0.02	-0.02
A	20	2	13	15	203.01	-0.01	-0.25
B	22	2	73	75	203.05	0.19	-0.09
A	20	2	19	21	203.07	-0.05	-0.28
A	20	2	25	27	203.13	-0.08	-0.22
B	22	2	85	87	203.17	0.08	0.16
A	20	2	31	33	203.19	-0.04	-0.21
A	20	2	37	39	203.25	-0.06	-0.13
B	22	2	97	99	203.29	0.13	0.13
A	20	2	43	45	203.31	0.04	-0.11
B	22	2	103	105	203.35	0.17	0.14
A	20	2	49	51	203.37	0.14	-0.06
B	22	2	109	111	203.41	0.33	0.14
A	20	2	55	57	203.43	0.24	-0.02
B	22	2	115	117	203.47	0.24	0.14
A	20	2	61	63	203.49	0.16	-0.13
B	22	2	121	123	203.53	0.27	0.22
A	20	2	67	69	203.55	0.30	0.04
B	22	2	127	129	203.59	0.12	0.24
A	20	2	73	75	203.61	0.35	-0.03
A	20	2	79	81	203.67	0.26	0.03
B	22	2	139	141	203.71	0.19	0.10
A	20	2	85	87	203.73	0.27	-0.01
B	22	2	145	147	203.77	0.20	0.06
A	20	2	91	93	203.79	0.16	-0.05
B	22	3	1	3	203.83	0.16	0.11
B	22	3	7	9	203.89	0.09	0.05
A	20	2	103	105	203.91	0.32	0.00
A	20	2	109	111	203.97	0.43	0.02
B	22	3	19	21	204.01	0.18	0.03
A	20	2	115	117	204.03	0.10	0.05
A	20	2	121	123	204.09	0.29	0.02
A	20	2	127	129	204.15	0.23	0.06
B	22	3	37	39	204.19	0.09	0.06
A	20	2	133	135	204.21	0.07	0.05
A	20	2	139	141	204.27	0.27	0.20
A	20	2	145	147	204.33	0.21	0.18
A	20	3	1	3	204.39	0.27	0.22
A	20	3	7	9	204.45	0.25	0.18
A	20	3	13	15	204.51	0.37	0.02

A	20	3	19	21	204.57	0.28	0.34
A	20	3	25	27	204.63	0.24	0.25
A	20	3	31	33	204.69	0.30	0.19
B	22	3	91	93	204.73	0.28	-0.60
B	22	3	97	99	204.79	0.20	-0.03
A	20	3	43	45	204.81	0.31	0.19
B	22	3	103	105	204.85	0.12	-0.02
B	22	3	115	117	204.97	0.15	0.08
B	22	3	121	123	205.03	0.21	-0.09
B	22	3	127	129	205.09	0.13	-0.02
B	22	3	133	135	205.15	0.07	-0.18
B	22	3	139	141	205.21	-0.02	-0.07
B	22	3	145	147	205.27	-0.01	-0.11
B	22	4	1	3	205.33	-0.02	-0.22
B	22	4	7	9	205.39	0.06	-0.18
B	22	4	13	15	205.45	-0.03	-0.01
B	22	4	19	21	205.51	0.06	-0.05
B	22	4	25	27	205.57	0.10	-0.06
B	22	4	31	33	205.63	0.15	0.03
B	22	4	37	39	205.69	0.18	-0.07
B	22	4	43	45	205.75	0.22	-0.04
B	22	4	49	51	205.81	0.22	-0.03
B	22	4	55	57	205.87	0.15	0.15
B	22	4	61	63	205.93	0.26	0.20
B	22	4	67	69	205.99	0.29	0.10
B	22	4	73	75	206.05	0.25	-0.08
B	22	4	79	81	206.11	0.31	0.24
B	22	4	85	87	206.17	0.28	0.03
B	22	4	91	93	206.23	0.30	0.02
B	22	4	97	99	206.29	0.28	0.05
B	22	4	103	105	206.35	0.30	-0.06
B	22	4	115	117	206.47	0.22	0.00
B	22	4	121	123	206.53	0.19	0.02
B	22	4	127	129	206.59	0.22	0.04
B	22	4	133	135	206.65	0.21	0.04
B	22	4	139	141	206.71	0.19	-0.09
B	22	4	145	147	206.77	0.22	0.14
B	22	5	1	3	206.83	0.22	0.05
B	22	5	7	9	206.89	0.31	-0.33
B	22	5	13	15	206.95	0.27	0.00
B	22	5	19	21	207.01	0.23	-0.12
B	22	5	31	33	207.13	0.18	-0.06
B	22	5	37	39	207.19	0.28	-0.20
B	22	5	49	51	207.31	0.17	-0.10
B	22	5	55	57	207.37	0.25	-0.20
B	22	5	61	63	207.43	0.38	-0.14
B	22	5	67	69	207.49	0.14	-0.04
B	22	5	73	75	207.55	0.17	-0.17

B	22	5	79	81	207.61	0.21	-0.08
B	22	5	85	87	207.67	0.15	-0.04
B	22	5	91	93	207.73	0.20	-0.07
B	22	5	97	99	207.79	0.20	-0.04
B	22	5	103	105	207.85	0.08	-0.09
B	22	5	109	111	207.91	0.30	0.04
B	22	5	115	117	207.97	0.09	-0.03
B	22	5	121	123	208.03	0.28	0.06
B	22	5	127	129	208.09	0.11	0.01
B	22	5	133	135	208.15	0.20	0.10
B	22	5	139	141	208.21	0.25	-0.06
B	22	5	145	147	208.27	0.19	0.13
B	22	6	1	3	208.33	0.24	0.01
B	22	6	7	9	208.39	0.24	0.07
B	22	6	13	15	208.45	0.16	0.08
B	22	6	19	21	208.51	0.09	0.19
B	22	6	25	27	208.57	0.26	0.07
B	22	6	31	33	208.63	0.21	0.04
B	22	6	37	39	208.69	0.14	0.02
B	22	6	49	51	208.81	0.26	-0.09
B	22	6	61	63	208.93	0.28	0.17
A	21	1	0	2	208.98	0.19	0.05
A	21	1	12	14	209.1	0.17	0.02
A	21	1	24	26	209.22	0.19	0.11
B	22	6	103	105	209.35	0.30	0.02
A	21	1	42	44	209.4	0.17	0.08
B	22	6	109	111	209.41	0.26	0.04
A	21	1	49	51	209.47	0.20	0.21
B	22	6	115	117	209.47	0.25	0.03
A	21	1	55	57	209.53	0.16	0.22
A	21	1	61	63	209.59	0.04	0.06
B	22	6	127	129	209.59	0.19	-0.12
A	21	1	67	69	209.65	0.21	0.22
A	21	1	73	75	209.71	0.18	0.16
A	21	1	79	81	209.77	0.34	0.13
A	21	1	85	87	209.83	0.28	0.22
A	21	1	91	93	209.89	0.27	0.16
A	21	1	97	99	209.95	0.87	-0.11
A	21	1	103	105	210.01	0.24	0.21
A	21	1	109	111	210.07	0.41	0.05
A	21	1	115	117	210.13	0.26	0.26
A	21	1	121	123	210.19	0.30	0.16
A	21	1	127	129	210.25	0.30	0.13
A	21	1	139	141	210.37	0.36	-0.06
A	21	1	145	147	210.43	0.31	0.13
A	21	2	1	3	210.49	0.11	0.01
A	21	2	7	9	210.55	0.25	0.13
A	21	2	13	15	210.61	0.19	0.08

A	21	2	19	21	210.67	0.04	0.06
A	21	2	25	27	210.73	0.18	0.09
A	21	2	31	33	210.79	0.25	0.07
A	21	2	37	39	210.85	0.29	0.15
A	21	2	43	45	210.91	0.31	0.21
A	21	2	49	51	210.97	0.29	0.15
A	21	2	55	57	211.03	0.16	0.04
A	21	2	61	63	211.09	0.30	0.21
A	21	2	67	69	211.15	0.40	0.17
A	21	2	73	75	211.21	0.24	0.21
A	21	2	79	81	211.27	0.23	0.18
A	21	2	85	87	211.33	0.33	0.19
A	21	2	91	93	211.39	0.24	0.10
A	21	2	103	105	211.51	0.25	0.09
A	21	2	105	107	211.53	0.32	0.14
A	21	2	115	117	211.63	0.26	0.21
A	21	2	121	123	211.69	0.30	0.21
A	21	2	133	135	211.81	0.35	0.18
A	21	3	1	3	211.99	0.16	0.02
A	21	3	7	9	212.05	0.28	0.04
A	21	3	25	27	212.23	0.10	0.04
A	21	3	31	33	212.29	0.37	0.02
A	21	3	37	39	212.35	0.35	0.05
A	21	3	55	57	212.53	0.24	0.00
A	21	3	61	63	212.59	0.28	-0.01
A	21	3	67	69	212.65	0.44	-0.03
A	21	3	73	75	212.71	0.24	0.11
A	21	3	79	81	212.77	0.35	-0.02
A	21	3	109	111	213.07	0.29	0.02
A	21	3	115	117	213.13	0.17	-0.08
A	21	3	121	123	213.19	0.16	-0.14
A	21	3	127	129	213.25	0.16	-0.13
A	21	3	133	135	213.31	0.09	-0.10
A	21	3	139	141	213.37	0.08	-0.17
A	21	3	145	147	213.43	0.17	-0.09
A	21	4	1	3	213.49	0.15	-0.10
A	21	4	7	9	213.55	0.12	-0.04
A	21	4	13	15	213.61	0.24	-0.01
A	21	4	19	21	213.67	0.24	-0.12
A	21	4	25	27	213.73	0.22	0.09
A	21	4	31	33	213.79	0.17	0.04
A	21	4	37	39	213.85	0.24	0.04
A	21	4	43	45	213.91	0.29	0.05
A	21	4	49	51	213.97	0.38	0.04
A	21	4	55	57	214.03	0.31	0.11
A	21	4	61	63	214.09	0.29	0.15
A	21	4	67	69	214.15	0.32	0.17
A	21	4	73	75	214.21	-0.06	0.22

A	21	4	79	81	214.27	0.38	0.09
A	21	4	85	87	214.33	0.25	0.06
A	21	4	91	93	214.39	-0.08	-0.16
A	21	4	97	99	214.45	0.09	0.07
A	21	4	103	105	214.51	0.22	0.19
A	21	4	109	111	214.57	0.23	0.10
A	21	4	115	117	214.63	0.24	0.16
A	21	4	121	123	214.69	0.26	0.30
A	21	4	127	129	214.75	0.10	0.15
A	21	4	133	135	214.81	0.29	0.13
A	21	4	139	141	214.87	0.37	0.11
A	21	4	145	147	214.93	0.43	0.15
A	21	5	1	3	214.99	0.25	0.23
B	23	2	49	51	215.05	0.20	0.18
A	21	5	7	9	215.05	0.30	0.12
A	21	5	13	15	215.11	0.28	0.07
B	23	2	55	57	215.11	0.45	0.15
A	21	5	19	21	215.17	0.31	0.14
B	23	2	61	63	215.17	0.38	0.08
B	23	2	67	69	215.23	-0.86	-2.08
A	21	5	25	27	215.23	0.35	-0.03
B	23	2	73	75	215.29	0.29	0.19
A	21	5	31	33	215.29	0.38	0.05
A	21	5	37	39	215.35	0.30	-0.02
B	23	2	79	81	215.35	0.37	0.05
A	21	5	43	45	215.41	0.20	0.21
B	23	2	85	87	215.41	0.21	0.04
A	21	5	49	51	215.47	0.22	0.03
B	23	2	91	93	215.47	0.25	0.01
B	23	2	97	99	215.53	0.21	0.05
B	23	2	103	105	215.59	0.16	-0.11
B	23	2	109	111	215.65	0.15	0.05
B	23	2	115	117	215.71	0.18	-0.52
B	23	2	121	123	215.77	0.29	0.19
B	23	2	127	129	215.83	0.07	-0.08
B	23	2	133	135	215.89	0.16	0.00
B	23	2	139	141	215.95	0.09	-0.05
B	23	2	145	147	216.01	0.15	-0.01
B	23	3	1	3	216.07	0.15	-0.06
B	23	3	7	9	216.13	0.18	0.24
B	23	3	13	15	216.19	0.13	0.07
B	23	3	19	21	216.25	0.24	0.28
B	23	3	37	39	216.43	0.29	0.27
B	23	3	43	45	216.49	0.20	0.24
B	23	3	49	51	216.55	0.16	0.20
B	23	3	55	57	216.61	0.29	0.26
B	23	3	61	63	216.67	0.19	0.20
B	23	3	67	69	216.73	0.18	0.19

B	23	3	73	75	216.79	0.21	0.11
B	23	3	79	81	216.85	0.30	0.03
B	23	3	85	87	216.91	0.16	0.08
B	23	3	91	93	216.97	0.25	0.09
B	23	3	97	99	217.03	0.16	0.10
B	23	3	103	105	217.09	0.20	-0.03
B	23	3	109	111	217.15	0.16	0.07
B	23	3	115	117	217.21	0.26	0.10
B	23	3	121	123	217.27	0.20	0.16
B	23	3	127	129	217.33	0.21	0.18
B	23	3	133	135	217.39	0.28	0.15
B	23	3	139	141	217.45	0.28	0.24
B	23	3	145	147	217.51	0.28	0.21
B	23	4	1	3	217.57	0.36	0.17
B	23	4	7	9	217.63	0.19	0.16
B	23	4	13	15	217.69	0.23	0.20
B	23	4	19	21	217.75	0.16	0.21
B	23	4	25	27	217.81	0.22	0.06
B	23	4	31	33	217.87	0.15	0.16
B	23	4	43	45	217.99	0.05	0.12
B	23	4	55	57	218.11	0.36	-0.12
B	23	4	61	63	218.17	0.37	0.14
B	23	4	73	75	218.29	0.36	0.10
B	23	4	79	81	218.35	0.32	0.11
B	23	4	85	87	218.41	0.30	0.06
B	23	4	91	93	218.47	0.16	0.13
B	23	4	97	99	218.53	0.23	0.01
B	23	4	103	105	218.59	0.24	0.15
B	23	4	109	111	218.65	0.27	0.12
B	23	4	115	117	218.71	0.18	0.11
B	23	4	121	123	218.77	0.04	-0.19
B	23	4	127	129	218.83	0.19	0.10
B	23	4	133	135	218.89	0.29	0.09
B	23	4	139	141	218.95	0.14	0.11
B	23	4	145	147	219.01	0.16	0.13
B	23	5	1	3	219.07	0.19	0.11
B	23	5	7	9	219.13	0.11	0.14
B	23	5	13	15	219.19	0.26	0.14
B	23	5	19	21	219.25	0.25	0.12
B	23	5	25	27	219.31	0.02	0.04
B	23	5	31	33	219.37	0.06	0.06
B	23	5	37	39	219.43	0.21	-0.04
B	23	5	43	45	219.49	0.27	0.01
B	23	5	49	51	219.55	0.25	0.11
B	23	5	55	57	219.61	0.01	-0.05
B	23	5	61	63	219.67	0.18	-0.01
B	23	5	67	69	219.73	0.04	-0.05
B	23	5	73	75	219.79	0.10	-0.07

B	23	5	79	81	219.85	0.20	-0.09
B	23	5	85	87	219.91	0.07	0.02
B	23	5	91	93	219.97	0.16	-0.05
B	23	5	97	99	220.03	0.04	-0.11
A	22	1	67	69	220.04	0.20	0.18
B	23	5	103	105	220.09	0.09	-0.07
A	22	1	73	75	220.1	0.25	-0.05
A	22	1	79	81	220.16	0.12	-0.10
A	22	1	85	87	220.22	0.16	0.05
A	22	1	97	99	220.34	0.16	0.14
A	22	1	103	105	220.4	0.23	0.03
A	22	1	109	111	220.46	0.26	0.02
A	22	1	115	117	220.52	0.19	-0.10
A	22	1	121	123	220.58	0.17	-0.06
A	22	1	127	129	220.64	0.07	-0.11
A	22	2	7	9	220.74	0.15	-0.16
A	22	2	13	15	220.8	0.13	-0.03
A	22	2	19	21	220.86	0.17	-0.14
A	22	2	31	33	220.98	0.27	0.02
A	22	2	37	39	221.04	0.10	-0.10
A	22	2	43	45	221.1	0.31	0.07
A	22	2	49	51	221.16	0.25	0.14
A	22	2	55	57	221.22	0.29	0.05
A	22	2	61	63	221.28	0.22	0.06
A	22	2	67	69	221.34	0.27	0.14
A	22	2	73	75	221.4	0.18	0.20
A	22	2	85	87	221.52	0.27	0.24
A	22	2	97	99	221.64	0.17	0.09
A	22	2	109	111	221.76	0.18	0.02
A	22	2	115	117	221.82	0.12	-0.03
A	22	2	121	123	221.88	0.10	-0.15
A	22	2	127	129	221.94	0.16	-0.04
A	22	2	133	135	222	0.22	-0.23
A	22	2	139	141	222.06	0.24	0.01
A	22	2	145	147	222.12	0.23	-0.06
A	22	3	1	3	222.18	0.28	-0.03
A	22	3	13	15	222.3	0.28	-0.03
A	22	3	25	27	222.42	0.38	-0.08
A	22	3	31	33	222.48	0.27	0.08
A	22	3	37	39	222.54	0.24	0.20
A	22	3	43	45	222.6	0.28	0.05
A	22	3	49	51	222.66	0.38	0.06
A	22	3	55	57	222.72	0.26	0.02
A	22	3	67	69	222.84	0.32	-0.05
A	22	3	73	75	222.9	0.28	0.03
A	22	3	79	81	222.96	0.33	0.08
A	22	3	91	93	223.08	0.29	-0.06
A	22	3	103	105	223.2	0.18	-0.12

A	22	3	109	111	223.26	0.24	0.05
A	22	3	115	117	223.32	0.33	-0.04
A	22	3	121	123	223.38	0.34	0.09
A	22	4	1	3	223.68	0.33	0.02
A	22	4	19	21	223.86	0.32	0.09
B	24	4	31	33	226.2	0.29	-0.07
B	24	4	37	39	226.26	0.27	0.02
B	24	4	43	45	226.32	0.23	-0.06
B	24	4	49	51	226.38	0.32	-0.14
B	24	4	55	57	226.44	0.23	0.16
B	24	4	61	63	226.5	0.15	-0.04
B	24	4	67	69	226.56	0.11	0.00
B	24	4	73	75	226.62	0.19	-0.05
B	24	4	79	81	226.68	0.29	-0.25
B	24	4	85	87	226.74	0.14	0.03
B	24	4	91	93	226.8	-0.07	-0.11
B	24	4	97	99	226.86	0.09	-0.01
B	24	4	103	105	226.92	0.30	-0.09
B	24	4	109	111	226.98	0.10	-0.09
B	24	4	115	117	227.04	0.10	-0.09
B	24	4	121	123	227.1	0.18	-0.09
B	24	4	127	129	227.16	0.13	0.03
B	24	4	133	135	227.22	0.18	-0.02
B	24	4	139	141	227.28	0.18	-0.08
B	24	4	145	147	227.34	0.22	0.14
B	24	5	1	3	227.4	0.27	0.05
B	24	5	7	9	227.46	0.29	0.11
B	24	5	13	15	227.52	0.41	0.16
B	24	5	19	21	227.58	0.36	0.30
B	24	5	25	27	227.64	0.29	0.06
B	24	5	31	33	227.7	0.27	0.10
B	24	5	37	39	227.76	0.32	0.06
B	24	5	43	45	227.82	0.22	0.12
B	24	5	49	51	227.88	0.26	-0.01
B	24	5	55	57	227.94	0.36	0.18
B	24	5	61	63	228	0.32	-0.19
B	24	5	67	69	228.06	0.27	0.00
B	24	5	73	75	228.12	0.19	-0.18
B	24	5	79	81	228.18	0.23	-0.09
B	24	5	85	87	228.24	0.27	0.20
B	24	5	91	93	228.3	0.33	-0.01
B	24	5	97	99	228.36	0.17	-0.06
B	24	5	103	105	228.42	0.26	-0.08
B	24	5	109	111	228.48	0.22	-0.09
B	24	5	115	117	228.54	0.21	-0.10
B	24	5	121	123	228.6	0.27	-0.06
B	24	5	127	129	228.66	0.27	-0.15
B	24	5	133	135	228.72	0.26	-0.08

B	24	5	139	141	228.78	0.06	-0.07
B	24	5	145	147	228.84	0.16	-0.15
B	24	6	1	3	228.9	0.32	-0.01
B	24	6	7	9	228.96	0.23	0.04
B	24	6	13	15	229.02	0.14	-0.23
B	24	6	19	21	229.08	0.24	-0.03
B	24	6	25	27	229.14	0.17	-0.15
B	24	6	31	33	229.2	0.17	0.01
B	24	6	37	39	229.26	0.23	-0.07
B	24	6	43	45	229.32	0.24	-0.03
B	24	6	49	51	229.38	0.24	-0.05
B	24	6	55	57	229.44	0.26	0.07
B	24	6	61	63	229.5	0.30	0.01
B	24	6	67	69	229.56	0.20	0.01
B	24	6	73	75	229.62	0.31	0.04
B	24	6	79	81	229.68	0.11	0.15
B	24	6	85	87	229.74	0.22	0.12
B	24	6	91	93	229.8	0.19	0.09
B	24	6	97	99	229.86	0.38	0.02
B	24	6	103	105	229.92	0.38	0.07
B	24	6	109	111	229.98	0.29	0.14
B	24	6	115	117	230.04	0.51	0.07
B	24	7	7	9	230.17	0.26	0.05
B	24	7	13	15	230.23	0.20	0.06
B	24	7	19	21	230.29	0.44	0.10
B	24	7	25	27	230.35	0.32	-0.01
B	24	7	31	33	230.41	0.22	0.10
B	24	7	37	39	230.47	0.26	0.02
B	24	7	43	45	230.53	0.32	0.08
B	24	7	49	51	230.59	0.28	0.08
B	24	8	1	3	230.65	0.19	0.04
B	24	8	7	9	230.71	0.25	0.06
B	24	8	13	15	230.77	0.22	0.08
B	24	8	19	21	230.83	0.31	0.05
B	24	8	25	27	230.89	0.29	0.16
B	24	8	31	33	230.95	0.19	-0.01
B	24	8	37	39	231.01	0.17	-0.08
B	25	1	79	81	234.42	0.27	0.02
B	25	1	85	87	234.48	0.25	-0.03
B	25	1	91	93	234.54	0.24	0.00
B	25	1	97	99	234.6	0.21	-0.21
B	25	1	103	105	234.66	0.28	-0.11
B	25	1	109	111	234.72	0.38	-0.07
B	25	1	121	123	234.84	0.29	-0.06
B	25	1	127	129	234.9	0.32	-0.12
B	25	1	133	135	234.96	0.74	0.20
B	25	1	139	141	235.02	0.21	-0.04
B	25	1	145	147	235.08	0.21	0.00

B	25	2	1	3	235.14	0.18	-0.20
B	25	2	7	9	235.2	0.29	0.05
B	25	2	13	15	235.26	0.25	-0.02
B	25	2	19	21	235.32	0.22	-0.04
B	25	2	25	27	235.38	0.13	-0.21
B	25	2	31	33	235.44	0.30	-0.17
B	25	2	43	45	235.56	0.20	-0.21
B	25	2	49	51	235.62	0.15	-0.23
B	25	2	55	57	235.68	0.09	-0.31
B	25	2	61	63	235.74	0.10	-0.17
B	25	2	67	69	235.8	0.31	-0.01
B	25	2	79	81	235.92	0.50	-0.24
B	25	2	85	87	235.98	0.39	0.00
B	25	2	91	93	236.04	0.54	0.00
B	25	2	97	99	236.1	0.30	0.03
B	25	2	103	105	236.16	0.44	0.12
B	25	2	109	111	236.22	0.46	0.14
B	25	2	115	117	236.28	0.27	0.07
B	25	2	121	123	236.34	0.39	0.00
B	25	2	127	129	236.4	0.40	0.08
B	25	2	133	135	236.46	0.28	-0.07
B	25	2	139	141	236.52	0.05	0.06
B	25	2	145	147	236.58	0.27	0.03
B	25	3	19	21	236.82	0.39	-0.16
B	25	3	31	33	236.94	0.20	0.00

TABLE 2. Benthic foraminiferal trace element records for site 1408

HOLE	CORE	SECTION	TOP_DEPTH	BOTTOM_DEPTH	MCD(m)	Mg/Ca (mmol/mol)	B/Ca (umol/mol)
B	19	3	1	3	168.79	0.741093038	121.7601563
B	19	3	7	9	168.85		
B	19	3	43	45	169.21	0.773855435	129.3107644
B	19	3	55	57	169.33	0.73486968	127.3332828
B	19	3	79	81	169.57	0.739803268	128.1824182
B	19	3	133	135	170.11	0.712965717	119.1222612
B	19	4	25	27	170.53	0.772368699	123.1679781
A	17	2	115	117	173.63	0.766180004	112.1453321
A	17	2	127	129	173.75	0.624955655	123.5232324
A	17	2	139	141	173.87	0.867871977	118.1837096
A	17	2	145	147	173.93	0.761139433	114.7952118
A	17	3	7	9	174.05	1.28232656	139.4881813
A	17	3	13	15	174.11	0.96777148	112.3671788
A	17	3	19	21	174.17	0.718327385	119.4831976
A	17	3	31	33	174.29	0.650475359	114.6135507
A	17	3	37	39	174.35	0.668916317	126.4515355
A	17	3	43	45	174.41	0.764141006	128.8555238
A	17	3	55	57	174.53	0.739951666	122.2671479
A	17	3	61	63	174.59	0.910138923	111.2640887
A	17	3	67	69	174.65	1.041224565	107.0084696
A	17	3	73	75	174.71	1.014633068	101.9876874
A	17	3	85	87	174.83	0.772235941	122.8599469
A	17	3	103	105	175.01	1.395839944	158.0073123
A	17	3	121	123	175.19	0.987558179	132.9153466
A	17	4	1	3	175.49	0.927724603	116.9283616
A	17	4	19	21	175.67	0.852138594	114.3274229
A	17	4	31	33	175.79	0.874408052	114.5492605
A	17	4	55	57	176.03	0.981257742	113.9930421
A	17	4	79	81	176.27	0.973578205	121.5377179
A	17	4	91	93	176.39	1.005944057	117.0478773
A	17	4	115	117	176.63	0.938223695	122.6066977
A	17	4	139	141	176.87	1.010172003	124.0270818
A	17	5	1	3	176.99	1.025737969	125.8568488
A	17	5	13	15	177.11	1.273619931	114.2662381
A	17	5	25	27	177.23	1.024198251	109.6486602
A	17	5	49	51	177.47	0.947648785	115.8271288
A	17	5	73	75	177.71	0.739763437	99.73132864
A	17	5	85	87	177.83	1.005598667	119.4118597

A	17	5	103	105	178.01	1.036911457	116.7572165
B	21	2	121	123	191.63	0.950282909	126.6040783
B	21	2	127	129	191.69	1.182830974	142.3882037
B	21	3	19	21	192.11	1.50295742	165.2036469
B	21	3	55	57	192.47	1.135028932	128.9027474
B	21	3	73	75	192.65	1.118666403	128.5940324
B	21	3	103	105	192.95	1.111654687	123.9740205
B	21	3	145	147	193.37	1.222395802	135.6558122
B	21	4	25	27	193.67	1.091346232	126.3782251
B	21	4	31	33	193.73		
B	21	4	49	51	193.91	1.32280102	133.0801446
B	21	4	73	75	194.15	1.410388755	158.6230301
B	21	5	1	3	194.93	1.142242989	121.6752116
B	21	5	25	27	195.17	1.524057134	179.5712353
B	21	5	49	51	195.41	1.064856211	113.9767832
B	21	5	67	69	195.59	1.4315651	156.9300036
B	21	5	109	111	196.01	1.601786757	191.2048961
B	21	6	19	21	196.61	1.119737803	120.9920461
B	21	6	25	27	196.67		
B	21	6	55	57	196.97	1.75174059	199.8158097
B	21	6	109	111	197.51	1.42893599	114.3367577
B	21	6	127	129	197.69	1.109798303	116.4731351
B	22	2	49	51	202.81	1.443075316	126.7879405
B	22	2	61	63	202.93	1.435694876	122.9050159
B	22	2	109	111	203.41	1.415978882	122.7354867
B	22	2	121	123	203.53	1.507739218	128.9242659
B	22	2	127	129	203.59		
B	22	3	7	9	203.89	1.555728363	129.5365745
B	22	4	1	3	205.33	1.294611629	115.4578566
B	22	4	7	9	205.39		
B	22	4	37	39	205.69	1.579330882	124.179165
B	22	4	61	63	205.93	1.447506512	115.9965477
B	22	4	67	69	205.99		
A	21	2	73	75	211.21	1.271127645	112.0465806
A	21	3	13	15	212.11	1.303216734	113.6951224
A	21	3	139	141	213.37	1.16471973	95.59922118
A	21	3	145	147	213.43		
A	21	4	31	33	213.79	1.472167479	120.6524191
A	21	4	37	39	213.85		
A	21	4	109	111	214.57	1.677458481	124.6198255

A	22	1	103	105	220.4	2.027432053	162.5886648
A	22	1	109	111	220.46		
A	22	1	127	129	220.64	1.441993665	117.7682911
A	22	2	115	117	221.82	1.328961907	110.3848574
B	24	4	103	105	226.92	1.602046569	131.686397
B	24	4	109	111	226.98		
B	24	5	7	9	227.46	1.721036181	126.8927711
B	24	5	13	15	227.52		
B	24	5	37	39	227.76	1.343087067	104.3229953
B	24	5	43	45	227.82		
B	24	5	103	105	228.42	1.658509646	122.8115665
B	24	6	49	51	229.38	1.668243335	128.6076819
B	24	7	31	33	230.41	1.826258773	141.0094288

Table 3. Data of standards in stable isotope runs

	CM12		NBS18		NBS19	
run date	**$\delta^{13}C$ source corrected**	**$\delta^{18}O$ source corrected**	**$\delta^{13}C$ source corrected**	**$\delta^{18}O$ source corrected**	**$\delta^{13}C$ source corrected**	**$\delta^{18}O$ source corrected**
140129	2.07	-1.96	-5.03	-23.00	1.96	-2.24
	2.03	-1.95	-4.99	-23.02	1.94	-2.07
	2.02	-1.92				
	2.06	-1.87				
	2.08	-2.06				
140303	2.07	-2.04	-5.03	-23.02	1.93	-2.20
	2.02	-1.91	-4.99	-23.00	1.92	-2.13
	2.10	-1.90				
	2.04	-1.96				
	2.13	-1.92				
140410	2.09	-1.96	-4.99	-22.98	1.93	-2.27
	2.07	-1.90	-5.03	-23.04	1.93	-2.16
	2.10	-1.79				
	2.02	-1.94				
140714	2.09	-1.99	-5.21	-23.55	1.92	-2.16
	2.08	-1.90	-4.81	-22.47	1.96	-2.19
	2.04	-1.93				
	2.05	-1.94				
	2.03	-1.91				
140808	2.13	-2.04	-4.92	-22.87	1.97	-2.19
	2.09	-1.95	-5.01	-23.05	1.91	-2.11
	2.01	-1.97	-5.05	-23.05		
	2.04	-1.96	-5.06	-23.07		
	2.03	-1.89				
140814	2.16	-2.01	-5.03	-22.99	1.94	-2.14
	2.07	-1.97	-5.05	-23.09	1.93	-2.16
	2.04	-1.98	-5.02	-22.95	1.92	-2.14
	2.00	-1.96	-4.94	-23.02		
	2.07	-1.90				
140820	2.08	-1.94	-5.03	-23.04	1.93	-2.17
	2.10	-1.90	-4.99	-22.98	1.94	-2.22
	2.05	-1.91				
	2.07	-1.83				
	2.04	-1.97				

140828	2.16	-2.02	-4.98	-23.08	1.91	-2.14
	2.04	-1.94	-5.03	-22.94	1.95	-2.18
	2.05	-1.86				
	2.06	-1.93				
	2.04	-2.01				
140905	2.07	-1.93	-5.01	-22.94	1.97	-2.17
	2.05	-1.99	-5.01	-23.08	1.91	-2.18
	2.04	-1.90				
	2.08	-1.91				
140908	2.11	-1.98	-4.99	-23.06	1.92	-2.27
	2.12	-1.87	-5.03	-22.96	1.90	-2.17
	2.08	-1.81				
	2.06	-1.86				
	2.07	-1.93				
140919	2.08	-2.00	-4.75	-22.92	1.94	-2.18
	2.12	-1.95	-5.27	-23.10	1.95	-2.09
	1.98	-2.15				
	2.10	-1.86				
	2.01	-1.88				
140924	1.97	-1.84	-4.95	-22.96	1.90	-2.35
	2.18	-1.81	-5.06	-23.05	1.95	-2.12
	2.10	-1.94				
	2.05	-1.91				
141006	2.07	-1.91	-4.95	-23.01	1.96	-2.18
	2.05	-1.92	-5.07	-23.01		
	2.01	-1.87				
	2.02	-2.01				
	2.06	-1.94				
141007	2.09	-2.00	-4.97	-23.02	1.93	-2.13
	2.08	-1.85	-5.05	-23.00	1.92	-2.24
	2.05	-1.92				
141017	2.04	-1.97	-4.98	-23.05	1.93	-2.20
	2.18	-1.94	-5.04	-22.97		
	2.07	-1.92				
	2.03	-1.82				
	2.02	-1.89				

141022	2.04	-1.85	-5.01	-23.09	1.96	-2.27
	2.12	-1.79	-5.01	-22.93	1.91	-2.19
	2.08	-1.87				
	2.06	-1.98				
	2.03	-1.91				
141028	2.07	-1.92	-4.99	-23.08	1.95	-2.12
	2.12	-1.95	-5.03	-22.94	1.90	-2.24
	2.07	-1.89				
	2.07	-2.02				
	2.05	-1.86				
141030	2.07	-1.93	-4.93	-22.99	1.99	-2.28
	2.12	-1.88	-5.09	-23.03	1.89	-2.13
	2.04	-1.92				
	2.09	-1.84				
	1.99	-1.96				
141104	2.05	-1.88	-4.97	-22.83	1.94	-2.23
	2.09	-1.84	-5.05	-23.19	1.95	-2.22
	2.08	-1.90				
	2.04	-1.89				
	2.01	-1.92				
141111	2.06	-1.85	-5.01	-23.01	2.08	-2.35
	2.13	-1.93			1.86	-2.08
	1.99	-1.85				
	1.98	-1.95				
	2.00	-1.91				
141117	2.06	-1.93	-4.93	-22.85		
	2.07	-1.70	-5.09	-23.17		
	2.01	-1.97				
	2.04	-2.03				
	2.07	-1.93				
141118	2.09	-1.94	-4.97	-23.10	1.94	-2.21
	2.05	-1.91	-5.05	-22.92	1.94	-2.16
	2.03	-1.91				
141122	2.04	-2.01	-5.01	-23.04	1.94	-2.06
	2.15	-1.96	-5.01	-22.98	1.92	-2.22
	2.02	-1.96				
	2.14	-2.05				
	2.02	-1.87				

141202	2.09	-1.92	-4.79	-22.99	1.99	-2.20
	2.06	-1.89	-5.23	-23.03	1.93	-2.19
	2.02	-1.84				
	2.00	-2.01				
141205	2.12	-1.86	-5.03	-23.06	1.95	-2.33
	2.11	-1.96	-4.99	-22.96	1.92	-2.15
	2.06	-1.81				
	2.01	-1.81				
	2.04	-1.90				
150505	1.98	-2.05	-5.01	-23.01	1.95	-2.20
	2.07	-1.96			1.97	-2.10
	2.00	-1.95				
	2.10	-1.87				
150506	2.01	-1.92	-5.01	-23.01	1.96	-2.21
	2.11	-1.86			1.92	-2.22
	2.07	-1.92				
	2.06	-1.87				
150514	2.09	-1.86	-4.98	-23.01	1.98	-2.20
	2.10	-1.91	-5.04	-23.01	1.92	-2.17
	2.05	-1.89				
	2.00	-2.03				
	2.01	-1.91				

	CM12		AtlanticII		NBS19	
run date	**$\delta^{13}C$ source corrected**	**$\delta^{18}O$ source corrected**	**$\delta^{13}C$ source corrected**	**$\delta^{18}O$ source corrected**	**$\delta^{13}C$ source corrected**	**$\delta^{18}O$ source corrected**
140512	2.04	-1.98	1.02	3.43	1.92	-2.19
	2.15	-1.91			1.92	-2.17
	2.01	-1.96				
	2.12	-1.86				
	2.06	-1.94				
140624	2.10	-1.92	0.81	3.48	1.86	-2.26
	2.06	-1.98	0.95	3.34	1.95	-2.16
	2.04	-1.86				
	2.18	-1.77				
	2.05	-1.97				
140707	2.11	-2.02	0.90	3.39	1.95	-2.12
	2.02	-1.92	0.84	3.43	1.93	-2.20
	2.09	-2.00				
	2.05	-1.90				
	2.02	-1.92				

	CM12		AtlanticII		LESVC	
run date	**$\delta^{13}C$ source corrected**	**$\delta^{18}O$ source corrected**	**$\delta^{13}C$ source corrected**	**$\delta^{18}O$ source corrected**	**$\delta^{13}C$ source corrected**	**$\delta^{18}O$ source corrected**
140417	2.02	-1.85	0.97	3.53	-46.53	-26.70
	2.03	-1.97	0.90	3.32	-46.67	-26.70
	2.08	-1.90				
140418	2.08	-1.83	0.99	3.46	-46.60	-26.70
	2.05	-1.83	0.93	3.54		
	2.03	-1.98				
	2.05	-2.00				
140425	2.08	-1.79	0.88	3.33	-46.58	-26.72
	2.09	-1.90	0.80	3.52	-46.62	-26.68
	2.02	-1.97				
	2.05	-1.96				
	2.01	-1.93				
140430	2.09	-1.75	0.92	3.43	-46.68	-26.74
	2.06	-2.04	0.85	3.45	-46.52	-26.66
	2.01					
	2.06	-2.03				
	2.02	-1.82				
140510	2.06	-1.86	0.84	3.44	-46.65	-26.67
	2.12	-2.02	0.93	3.43	-46.55	-26.73
	2.05	-1.92				
	2.00	-1.91				
	2.02	-1.84				